https://doi.org/10.5194/egusphere-2026-1898
Preprint. Discussion started: 18 May 2026

Canopy temperatures in computationally expensive crop models: A resource-efficient emulator approach applied in LPJmL (version 5.9.18)

Marie Hemmen[1,2], Heidi Webber[3,4], Werner von Bloh[1], Jens Heinke[1], and Christoph Müller[1]

[1]Potsdam Institute for Climate lmpact Research (PIK), Member of the Leibniz Association, P.O. Box 60 12 03, D-14412 Potsdam, Germany
[2]Humboldt-Universität zu Berlin (HU), Albrecht Daniel Thaer-Institut für Agrar- und Gartenbauwissenschaften, Berlin, Germany
[3]Leibniz Centre for Agricultural Landscape Research (ZALF), Müncheberg, Germany
[4]Institute of Environmental Sciences, Brandenburg University of Technology, Cottbus, Germany

Correspondence: Marie Hemmen (marie.hemmen@pik-potsdam.de)

Abstract. Crop yields are determined by multiple process chains that respond to environmental conditions. The very complex interactions between the different processes as well as the effects of isolated and combined process-level signals on final yields can be examined with process-based models. One of the key signals for crop development and growth dynamics is temperature, which is subject to change under global warming. While some crop models compute temperatures at the canopy level, others take 2 m air temperatures as input. However, the two temperatures can deviate significantly, potentially leading to different process responses when the less accurate 2 m air temperatures are used. This particularly applies to high-temperature processes that exhibit nonlinear dynamics and are very sensitive to small temperature variations. For global models, a major limitation is the computational resources required by suitable canopy temperature approaches. In this study we present computationally efficient emulators based on a complex energy balance approach (EBSC) to simulate daily mean and maximum canopy temperatures of twelve different crops. The emulators are statistical models that include six variables describing weather conditions and crop status. Furthermore, the emulators contain interaction terms to consider the response of canopy temperature on interactions between the variables. We apply and evaluate the emulators in the global, process-based Lund-Potsdam-Jena managed Land (LPJmL) model and show that the emulator approach reproduces observed canopy heating and cooling effects depending on the water and nitrogen status of wheat. Furthermore, we compare the simulated daily mean and daily maximum canopy temperatures of all twelve crops to a global dataset of ERA5 skin temperatures. We find that, for daily mean temperatures, 2 m air temperatures are the better approximation of skin temperatures than the simulated canopy temperatures, whereas for daily maximum temperatures simulated canopy temperatures consistently outperform 2 m air temperatures in terms of bias and nonunity slope. Our results indicate that heat effects are substantially underestimated with 2 m air temperatures, while they are significantly better captured with simulated canopy temperatures. This suggests that replacing the 2 m air temperature input by simulated canopy temperatures considerably improves the ability to model high temperature impacts on crop growth.

https://doi.org/10.5194/egusphere-2026-1898
Preprint. Discussion started: 18 May 2026

1 Introduction

Increasing temperature trends have had severe impacts on global agricultural production in the past and could have even more drastic impacts in the future (Asseng et al., 2015; Teixeira et al., 2013; Gourdji et al., 2013). Particularly the number and intensity of heatwaves are expected to increase in a warming climate (Li et al., 2021; Seneviratne et al., 2021; Coumou and Rahmstorf, 2012), which can have significant negative, nonlinear effects on crop yields (Schlenker and Roberts, 2009; Lobell et al., 2011; Porter and Gawith, 1999). For example, Miller et al. (2021) estimate average per-country losses of 10.3 % in agricultural output per year by the end of the century due to heatwaves in an RCP 4.5 (no adaptation) scenario.

Global process-based crop models are an important tool to understand the impacts of high temperatures on global crop yields, to analyze potential climatic threats to global food security, particularly for future conditions, and to identify potential adaptation measures. They describe different processes in plants and soils and dynamically simulate plant and soil properties accounting for daily growth conditions at each simulated location. To consider high temperature effects on crops, many include temperature-dependent processes (Wang et al., 2017). A special case is that of heat stress, in which responses result when a high temperature threshold is surpassed leading to negative and largely irreversible effects on growth or development of a crop resulting in reduced yields. These processes are determined by the actual temperatures in the plant tissue which are often assumed to be identical to 2 m air temperatures (that are available as an input to models), while more complex approaches directly simulate the temperature of the plant. For this, canopy temperatures, defined here as the temperatures at the top layer of the crop canopy, are of central interest. Depending on the climatic conditions, the water status of a crop and its canopy properties, canopy temperatures can deviate substantially from 2 m air temperatures (Siebert et al., 2014; Amani et al., 1996) that are typically measured above a grass surface. For example, in hot and dry climates, where the vapor pressure deficit can be very high, the canopy of irrigated wheat can be several degrees lower than the air temperature. In contrast, high net radiation and a low stomatal conductance, e.g. due to low water availability, can lead to heating of the canopy. These potential differences can introduce substantial errors, if modeled processes rely on near-surface air temperatures instead of the more accurate canopy temperatures.

Although different approaches to compute canopy temperatures have been established, many global crop models still use air temperatures for a number of reasons: Empirical approaches (EMP) are trained on historic conditions in specific regions and may perform very well under conditions they are developed under. However, their applicability in regions with different climatic conditions or in future projections with a changing climate is expected to be limited, particularly given the non-linear relationship between air temperatures and vapor pressure deficit (VPD), which is the difference between actual and saturated vapor pressure, over the range of temperatures that crop heat stress occurs. While simple energy balance approaches (EBN) considering all energy fluxes between the plant and its surrounding can react to unknown conditions and are computationally easy, though they have been shown to perform worse than the EMP models in comparison studies in semi-arid environments from Webber et al. (2017, 2018). This might be due to their simplification of assuming a neutral stability of the atmosphere and therewith allowing only little heat transfer between the crop canopy and the surrounding air (Webber et al., 2017). Mechanistic complex energy balance approaches correcting for the atmospheric stability (EBSC) can accommodate new conditions and they

https://doi.org/10.5194/egusphere-2026-1898
Preprint. Discussion started: 18 May 2026

have been found to perform best compared to EMP and EBN (Webber et al., 2017). However, they need high computational resources, which can be a limitation for resource intensive global simulations.

The objective of this work is to develop a robust canopy temperature modeling approach, that is resource efficient and can therefore be used in global-scale applications. We derive a simplified model that is based on an EBSC approach and can conveniently be included in global crop models. With this, we aim to provide a method that is suitable to compute daily canopy temperatures of different crops growing in different regions producing reliable results for both historic and future climatic conditions. The simplified model is validated by comparing its results to those of the original one and then applied in the global process-based Lund-Potsdam-Jena managed Land (LPJmL) model to evaluate how the embedded approach performs globally.

2 Methods

2.1 The underlying EBSC model

Webber et al. (2016) describe the EBSC approach, that has been implemented in the Scientific Impact assessment and Modeling Platform for Advanced Crop and Ecosystem management (SIMPLACE) modeling framework (Enders et al., 2023) and on which this work builds, in detail in their study. Here, we provide a brief summary.

The EBSC approach considers all energy fluxes between the plant and its surrounding while at the same time accounting for the stability conditions of the atmosphere. The energy balance can be expressed by

$$R_n = LE + H + G, \tag{1}$$

where R_n is the net radiation at the crop's surface, LE is the latent energy flux (due to evaporation), H the sensible heat flux (by convection), and G the soil heat flux (by conduction) (Webber et al., 2016; Monteith and Unsworth, 1990).

Following Monteith and Unsworth (1990), and Clawson et al. (1989), Eq. (1) can also be formulated as

$$T_c = T_a + \frac{(R_n - G)\cdot r_a}{\rho \cdot c_p} \frac{\gamma \cdot (1 + \frac{r_c}{r_a})}{\Delta + \gamma \cdot (1 + \frac{r_c}{r_a})} - \frac{(e_a^* - e_a)}{\Delta + \gamma \cdot (1 + \frac{r_c}{r_a})}, \tag{2}$$

where T_c is the canopy temperature, T_a is the air temperature, ρ and c_p are the density and the specific heat of the air, Δ the slope of the saturated vapour pressure curve, γ the psychometric constant, e_a and e_a^* the actual and saturated vapour pressure of the air, and r_c and r_a the canopy and aerodynamic surface resistances.

Webber et al. (2016) correct for the atmospheric stability in r_a, which means that effects of buoyant forces are considered. These depend on surface temperature, i.e. canopy temperature, resulting in an interdependence of r_a and T_c. As both are unknown, numeric approaches are needed to find a solution for r_a, or T_c, respectively. Webber et al. (2016) report that in their numeric approach using the Monin-Obukhov-Similarity Theory (MOST) and empirical stability correction factors, approximately 90% of the iterations converge and provide solutions for T_c (in the conditions tested). However, the iterations needed for convergence can require high computing capacity, which is a limitation for global models with considerably high computing costs. To solve this problem, we rebuilt the model from Webber et al. (2016) as a stand-alone model in R (Hemmen et al., 2026) and from this

https://doi.org/10.5194/egusphere-2026-1898
Preprint. Discussion started: 18 May 2026

derive emulators that can be used in global models, such as LPJmL.

As in Webber et al. (2016), our rebuilt model includes the simplification of computing a lower and an upper canopy temperature limit, where the transpiration rates of a crop are at its maximum and minimum. This simplification is helpful insofar as the value for the canopy resistance r_c only needs to be known for one of the two boundary cases, namely the lower temperature case $T_{c,L}$, for which it can be computed as described in Allen and Wright (1997):

$$r_{c,L} = \frac{r_1}{0.5 \cdot LAI}, \tag{3}$$

where LAI is the actively transpiring leaf area index and r_1 is the stomatal resistance of a single leaf with a reference value for a grass crop of approximately 100 s/m (under well-watered conditions). $T_{c,L}$ can then be computed using Eq. (2) and $r_{c,L}$. For the upper canopy temperature limit case $T_{c,U}$, r_c is assumed to reach infinity and thus Eq. (2) reduces to

$$T_{c,U} = T_a + \frac{(R_n - G) \cdot r_a}{\rho \cdot c_p}. \tag{4}$$

The canopy temperature is finally calculated by scaling between these two limits with a water stress factor K_{WS} (Eq. (5)), e.g. the relation of actual to optimal canopy conductance.

$$T_c = T_{c,L} + (1 - K_{WS}) \cdot (T_{c,U} - T_{c,L}) \tag{5}$$

2.2 EBSC input and modeling protocol

To generate a dataset for subsequent training of the emulators, we use the rebuilt, stand-alone EBSC model with which we compute values for the two canopy temperature limits. In order to receive a global coverage, we supply the EBSC model with a dataset of randomly distributed grid-cell-day combinations, which we generated in a preprocessing step. It comprises 90000 entries, each containing variable values describing the weather conditions and crop status. Each entry corresponds to a specific spatial cell (with a resolution of 0.5°) on a specific day (between the years 1910 and 2100), so the variables describe the state of that cell on that day.

The selection of cell-days was done based on weather data and crop-specific leaf area index (LAI) values of twelve different crop types (section 2.4 and Tab. A1), which was produced by global crop simulations with LPJmL. For this, we used version 5.9.18 with the standard configuration, in which all temperature related LPJmL processes are driven with near-surface air temperature (i.e. no canopy temperature was considered). The simulations were forced with global climate data from the Inter-Sectoral Impact Model Intercomparison Project simulation round 3 (ISIMIP3b) (Lange and Büchner, 2021). ISIMIP3b provides data for different future projections based on several Representative Concentration Pathways (RCPs) and socioeconomic scenarios. In order to take into account a wide range of weather conditions considering a potential high increase of global mean temperature, we drove the LPJmL model with both historic and future SSP5-RCP8.5 conditions using GFDL-ESM4 climate data. As first step in our selection, we only considered the global LAI output of 33 different days of the year (DOYs) per year from 11 randomly selected historical years (in sum 363 different DOYs between 1910 and 2010), and 40 different DOYs per year from 9 future years (in sum 360 different DOYs between 2020 and 2100). From this set of days, only

https://doi.org/10.5194/egusphere-2026-1898
Preprint. Discussion started: 18 May 2026

cell-days with LAI values of minimum 1.5 were retained, because the known soil temperature signals and effects on canopy temperature during early growth stages (Webber et al., 2016; Wall et al., 2013) are not accounted for in the considered EBSC model. From the derived sample, we excluded all cell-days with negative daily mean temperatures and shortwave downwelling radiation values smaller 50 W/m^2. The remaining sample was then finally reduced by a random selection of cell-days, which are shown in Figure B1.

We assembled a global dataset of the selected cell-days, combining weather data extracted from the same ISIMIP source as was used in the LPJmL simulations with crop-specific data (crop type and respective LAI) taken from the LPJmL output. When multiple simulated crops of a selected cell-day exhibited LAI values exceeding 1.5, we selected one crop randomly to supply the crop-specific input data. Values for maximum heights of the simulated crops, required to compute the aerodynamic resistances, were mainly derived from the USDA National Plant Germplasm System (National Plant Germplasm System, United States Department of Agriculture-Agricultural Research Service, 2025; Byrne et al., 2018) (see Table A1 in the appendix). The accession numbers of the used database records are listed in .csv files in the Supplement. As the EBSC model is based on net radiation (R_n), we converted the shortwave and longwave downwelling radiation data provided by ISIMIP as is done LPJmL:

$$R_{nl} = R_l - \sigma \cdot (T_a + 273.15)^4 \tag{6}$$

$$R_n = (1 - albedo_{green\ leaves}) \cdot R_s + R_{nl} \cdot \left(\frac{daylength}{24}\right), \tag{7}$$

where R_l is the incoming, R_{nl} the net longwave radiation flux, and R_s the incoming solar irradiance (all in W/m^2), σ the Stefan-Boltzmann constant (in W/(m^{2}K^4)), and T_a the air temperature (in °C). For the albedo of green leaves, we used a value of 0.18.

The transfer of ISIMIP near-surface wind speeds at 10 m to wind speeds at the canopy level needed in the EBSC model is performed at runtime and follows Allen and Wright (1997), as was done in Webber et al. (2016) and Enders et al. (2023).

Many modeled plant processes, especially those with continuous, linear temperature responses, use mean temperatures as inputs. In contrast, plant processes which have responses only beyond a threshold, such as heat stress, exhibit non-linear behavior in high temperature ranges. Here, consideration of daily absolute maximum temperature values is important (Porter and Gawith, 1999). We therefore use two different simulation setups. The initial scenario is driven by both daily and spatially averaged input values and used to obtain daily mean canopy temperature limits of the selected cell-days. In the second configuration, we replace daily, cell-specific mean near-surface air temperature input with maximum values (T_{max}) so that resulting canopy temperature limits approximate daily maxima. This is based on the assumption that the maximum canopy temperatures coincide with the maximum near-surface air temperatures. To keep the temperature and radiation variables consistent, we assume daily maximum air temperatures to occur at 3 pm and derive the radiation value at this time of day (R_{tmax}, Eq. 9) from the net radiation (R_n) by assuming a sinusoidal radiation curve with a radiation maximum (R_{max}) at noon (Eq. 8). For the computation of R_{max}, we multiply R_n with $24/daylength$ to calculate back the mean daytime shortwave downwelling radiation from the

https://doi.org/10.5194/egusphere-2026-1898
Preprint. Discussion started: 18 May 2026

dataset provided by ISIMIP, which is a mean over 24 hours including nighttime hours. Furthermore, we substitute daily mean VPD (VPD_{mean}) with VPD at T_{max} (VPD_{max}). Figure B1 shows the value distributions of all variables in the assembled dataset for both simulation setups.

$$R_{max} = R_n \cdot \left(\frac{24}{daylength}\right) \cdot \left(\frac{\pi}{2}\right) \tag{8}$$

$$R_{tmax} = R_{max} \cdot \sin\left(\frac{\pi}{daylength} \cdot (15 - t_s)\right), \tag{9}$$

with

$$t_s = \left(12 - \frac{daylength}{2}\right) \tag{10}$$

2.3 Emulation of the EBSC model

In the EBSC model described above (Sect. 2.1), canopy temperatures are simulated as a function of water stress lying between two temperature limits (Eq. (5)). In our work, we supply emulators for these (upper and lower) limits. When implementing the emulators in global models, canopy temperature can be computed by applying an internally calculated water stress factor used for scaling between these limits. A comparable direct response may have been obtained using a single emulator considering a water stress variable. However, retaining water-stress computation within the global model preserves methodological flexibility, whereas incorporating it as an emulator input would bind the model's internal computation to the particular stress formulation used for training.

For the emulation, we use regression models with lower and upper canopy temperature limits from the EBSC model output as dependent variables, respectively, and up to six regressors, namely radiation (R), near-surface air temperature (T), windspeed (W), vapour pressure deficit (VPD), leaf area index (LAI), and maximum height of the crop (H). The choice of the regressors was derived from the simplified equations for lower and upper canopy temperatures (Eq. (2) and Eg. (4)). Radiation and air temperature are variables on which the canopy temperature limits are directly dependent. The same applies to VPD, though it is only relevant for the lower canopy temperature limit as the dependence of canopy temperature on VPD vanishes for the upper limit case (see also Eq. (4)). Leaf area index and maximum height indirectly contribute to T_c as they are used to determine the lower limit's canopy resistance and the actual height of the crop, which in turn is used to calculate roughness and displacement lengths of the plants. The latter two, along with windspeed, are needed to calculate the aerodynamic resistances.

Webber et al. (2016) suggest, that simple empirical relationships derived from single variable linear regressions between canopy temperature deviations from air temperature and climate drivers (such as radiation) are not sufficient to explain the differences between canopy and air temperature and that multivariate, non-linear relationships may perform better. Therefore, we use a parametric model, with a cubic polynomial basis function, that has been shown to work for emulating grain yields by Franke

https://doi.org/10.5194/egusphere-2026-1898
Preprint. Discussion started: 18 May 2026

et al. (2020). As in Franke et al. (2020), we also include interaction terms, such as the interaction between radiation and near-surface air temperature (Eq. (11)). The emulators consist of 84 terms in the case of the lower canopy temperature emulator and 56 terms for the upper canopy temperature emulator. We tested whether some terms could be dropped without significantly reducing the goodness of fit with the *step* function from the stats package in R (Hastie and Pregibon, 1992; Venables and Ripley, 2002), which uses the Akaike information criterion. However, as most terms turned out to be relevant, we use the full equation for further applications. We derive the parameter values of the emulators by an ordinary least squares fit with the *lm* function from the same stats package in R (Chambers, 1992; Wilkinson and Rogers, 1973). For this, we use the same input data for the independent variables as was used to drive the EBSC model (Sect. 2.2) and the EBSC model results for lower and upper canopy temperature limits corresponding to this input data. As we applied two distinct setups for the EBSC simulations, we receive two parameter sets per emulator, i.e. per canopy temperature limit. The derived parameter values are listed in Table A3 and Table A4 in the appendix and only correspond to the set of variable units and conditions used for the regression, which is listed in Table A2.

$$
\begin{aligned}
T_{c,L} = {} & k_1 \\
& + k_2\, R + k_3\, T + k_4\, W + k_5\, VPD + k_6\, LAI + k_7\, H \\
& + k_8\, R^2 + k_9\, T^2 + k_{10}\, W^2 + ... \\
& + k_{14}\, R \cdot T + k_{15}\, R \cdot W + ... \\
& + k_{19}\, T \cdot W + k_{20}\, T \cdot VPD + ... \\
& ... \\
& + k_{28}\, LAI \cdot H \\
& + k_{29}\, R^3 + k_{30}\, T^3 + k_{31}\, W^3 + ... \\
& + k_{35}\, R^2 \cdot T + k_{36}\, R^2 \cdot W + ... \\
& + k_{40}\, T^2 \cdot R + k_{41}\, T^2 \cdot W + ... \\
& ... \\
& + k_{60}\, H^2 \cdot R + k_{61}\, H^2 \cdot T + ... \\
& + k_{65}\, R \cdot T \cdot W + k_{66}\, R \cdot T \cdot VPD + ... \\
& + k_{75}\, T \cdot W \cdot VPD + k_{76}\, T \cdot W \cdot LAI + ... \\
& ... \\
& + k_{84}\, VPD \cdot LAI \cdot H
\end{aligned}
\tag{11}
$$

https://doi.org/10.5194/egusphere-2026-1898
Preprint. Discussion started: 18 May 2026

2.4 LPJmL model

LPJmL is a global model that dynamically simulates natural vegetation, managed land, and the terrestrial hydrology. The three components are coupled by carbon, water, and nitrogen cycles and include various biogeochemical and biophysical processes. A comprehensive description of the model is provided by Schaphoff et al. (2018a), Schaphoff et al. (2018b), and von Bloh et al. (2018) with updates up to version 5.7.9 described in Wirth et al. (2024). Further model developments of version 5.9.18, which is used here as a basis, that have not been published include technical changes, such as a new formatting and file ending of configuration files, a change in soil heat transfer routines and numerous further improvements and minor bug fixes, which are documented in a `CHANGELOG.md` file as part of the source code publication (Hemmen et al., 2026). In this work, we focus on the agricultural modules of LPJmL, that simulate the development and growth of twelve different crops, namely temperate cereals (e.g. wheat), rice, maize, tropical cereals (e.g. millet), pulses (e.g. field pea), temperate roots (e.g. sugar beet), tropical roots (e.g. cassava), sunflower, soybean, groundnuts, rapeseed, and sugarcane (Schaphoff et al., 2018b). The emulator approach described in this work in principle works for all crops, meaning that the parameter values are not constrained to only some crops. However, the site-specific validation and analysis in this study focus on wheat.

Many crop growth and development processes in LPJmL are temperature dependent. One example is the photosynthesis rate, which is at its maximum for a certain temperature range and decreases if temperatures are too low or too high. Another example is the onset of senescence, that is triggered once a certain amount of phenological heat units has been accumulated. Before the canopy temperature emulation was made available in LPJmL, all temperature related processes were driven with near-surface air temperatures or soil temperatures.

2.5 EBSC emulators in LPJmL

As described in Sect. 2.3, this work provides emulators for a lower and an upper canopy temperature limit, which represent canopy temperatures at two extreme states of water stress. The upper canopy temperature limit is reached when the canopy resistance is very high, or the canopy conductance is close to zero, due to high water stress. The lower canopy temperature limit is reached when the crop experiences low water stress and fully transpires. The associated optimum canopy conductance $g_{c,opt}$ is the reciprocal of the lower limit's canopy resistance $r_{c,L}$ (see Eq. (3)). The final canopy temperature (Eq. (5)) is computed by scaling between these two limits with a water stress factor K_{WS}. In LPJmL, we use the internally computed canopy conductance $g_{c,LPJmL}$ as a proxy for the water stress K_{WS} by normalizing it with the optimum canopy conductance $g_{c,opt}$.

$$K_{WS} = \min\left(1, \frac{g_{c,LPJmL}}{g_{c,opt}}\right) \tag{12}$$

While not directly affected, the canopy conductance $g_{c,LPJmL}$ is impacted by temperature-dependent processes, such as the photosynthetic rate or the stress caused by nitrogen limitation. For simplicity, we use mean near-surface air temperature as input in these temperature-dependent processes. After computation of the final air temperature-based $g_{c,LPJmL}$, we derive the water

https://doi.org/10.5194/egusphere-2026-1898
Preprint. Discussion started: 18 May 2026

stress scaling factor K_{WS} to compute both daily mean and daily maximum canopy temperatures. In the following, canopy temperatures that have been computed within LPJmL are referred to as simulated instead of emulated canopy temperatures, as the scaling with K_{WS} has a significant impact on the final value and is independent from the emulation.

Since the training of the emulators is constrained to certain value ranges for some dependent variables, we use the same constraints in LPJmL. This means that if the values of the respective variables fall below certain conditions, we set the canopy temperature to the value of the near-surface air temperature of the respective grid cell and day. Since the validation of the emulators (Sect. 3.1) revealed that their performance is weak for low wind speeds, we additionally added a condition for wind speeds in LPJmL. An overview of the constraining conditions is given in Table 1. Additionally, we also set the value of the canopy temperature equal to the value of the air temperature if either the emulated lower canopy temperature limit exceeds the value of the emulated upper canopy temperature or if the simulated canopy temperature is 10 K higher or lower than the air temperature.

Table 1. Thresholds of different LPJmL variables used for the computation of canopy temperatures. If the values of the variables fall below their respective thresholds, daily (minimum/maximum) canopy temperatures are set to the values of the corresponding daily (minimum/maximum) near-surface air temperatures.

Variable	Thresholds
shortwave downwelling radiation	50 W/m^2
air temperature (mean or maximum)	0 °C
leaf area index	1.5 m^2/m^2
wind speed	1 m/s
upper T_c limit	lower T_c limit

2.6 LPJmL modeling protocol

For simulations with LPJmL, we use version 5.9.18 with the standard configuration. This version is based on the nitrogen version of LPJmL, that includes the terrestrial carbon and nitrogen cycle (Schaphoff et al., 2018b; von Bloh et al., 2018; Wirth et al., 2024). For both the creation of different model configurations and to start the simulations, as well as for some postprocessing steps of the LPJmL output, we use the open source R package *lpjmlkit* (Breier et al., 2024). We first conduct a 3500 year spin-up, in which only natural vegetation is simulated to reach a dynamic pre-historical equilibrium of vegetation distribution and corresponding carbon and nitrogen pools. Subsequently, land use is introduced by a second, 420 year long, spin-up. We then perform a series of site-specific simulation experiments to analyze and compare the simulated canopy temperatures to observational data from two experiments, namely the Hot Serial Cereal (HSC) experiment and the China Wheat experiment. The setup of the two experiments are described in Sect. 2.7. For the HSC simulations we use GFDL-ESM4 climate data provided by ISIMIP3b (Lange and Büchner, 2021) over the period from 1901 to 2002 and for the China Wheat simulations we use the same input data but over the years 1901 to 1983. The subsequent years are driven with the climate data from the respective experiments (see Sect. 2.7). Any inconsistencies in the time series due to the combination of two different data sets

https://doi.org/10.5194/egusphere-2026-1898
Preprint. Discussion started: 18 May 2026

are deemed to not matter much, as canopy temperatures depend only on short-lived conditions of the vegetation. Furthermore, we use prescribed sowing dates as given in the experiment documentations and include the respective experimental harvest dates by specifying consistent phenological heat unit (PHU) requirements. These have been computed with an adjusted version of the crop calenders application (Waha et al., 2012; Minoli et al., 2019). The HSC experiment provides up to three measured LAI values per treatment, which we use to calibrate simulated LAI values. Besides, the HSC simulations did not consider water or nitrogen limitation as is consistent with the experimental setup under which the data were recorded. The China Wheat simulations use two different levels of irrigation. In LPJmL, we try to match the experimental conditions by first simulating rainfed wheat, where crops are not irrigated and only water from precipitation is available, and secondly using an LPJmL internal setting for potential irrigation, where the applied water fulfills the plants' demands. Regarding nitrogen availability, we use three LPJmL configurations, which enable the simulation of plant growth under the condition that firstly only the nitrogen available in the soil and from N-depositions can be used, secondly mineral nitrogen fertilizer is applied according to the input file for the specific region, and thirdly the plant receives as much nitrogen as demanded. Regarding historical atmospheric N deposition and historical atmospheric CO_2 concentration, we use inputs from Yang and Tian (2022) and Büchner and Reyer (2022).

For the global simulations, we use GSWP3-ERA5 climate data provided by ISIMIP (Kim, 2017; Hersbach et al., 2018; Lange et al., 2025), atmospheric N deposition data from Lamarque et al. (2013) and historical atmospheric CO_2 concentrations from Friedlingstein et al. (2023) for simulations from 1901 to 2004. Only rainfed crops with unlimited fertilizer applications are simulated.

For all LPJmL simulations, we use historical land-use patterns generated with the LandInG toolbox (Ostberg et al., 2023).

2.7 Evaluation details and reference data

One challenge in choosing the polynomial type and the number of parameters for the emulation is to select them in such a way that the model's predictive performance is strong while avoiding overfitting of the model. We therefore provide a cross validation of the emulators. For this, we drive both EBSC model simulations and emulators with a validation dataset which is independent from the training data set and which has a size of 45000 data points. We created the validation dataset applying the same selection method as for the training data set, but on a separate subset (Sect. 2.2 and Sect. 2.3). We then use a linear regression of the emulated values on the values simulated with the EBSC model to evaluate the emulators' performances. First, we analyze the square root of the mean squared error ($RMSE_{rp}$, Eq. (13), Sect. 2.8). Additionally, we evaluate the regression's intercept and slope (Sect. 3.1, Fig. 1).

Furthermore, we analyze which value ranges of the different input data variables lead to emulated canopy temperatures that differ by more than 2 K from the EBSC canopy temperatures. For this, we first select the respective cell-days from the assembled input dataset showing these differences. We then compare the values of the different input variables, namely radiation, temperature, wind, VPD, LAI, and maximum height of the subset to the respective variable values of the whole input dataset by plotting cumulative density functions. These finally reveal differences in the distribution of the subset compared to the full set for each of the input variables (Sect. 3.1, Fig. 2).

https://doi.org/10.5194/egusphere-2026-1898
Preprint. Discussion started: 18 May 2026

For the site-specific evaluation of simulated maximum canopy temperatures in LPJmL (Sect. 3.2.1), we use data from two different experiments. Here, site-specific denotes the simulation of only those cells (with a spatial resolution of 0.5°) that include the experimental sites and that are driven with the respective site-based experimental data. For all inputs relevant for LPJmL that are not provided by the measurement-based inputs, such as data on nitrogen deposition, we use daily and spatially averaged values of the respective cells obtained from multiple sources (e.g. ISIMIP, as explained in more detail above). We only validate daily maximum canopy temperatures, as daily mean values are not included in the experimental data. Firstly, we use data from the Hot Serial Cereal (HSC) experiment, which was conducted in Maricopa (Arizona, USA) (Wall et al., 2011; White et al., 2011; Kimball et al., 2012, 2015; Ottman et al., 2012). A spring wheat cultivar was planted approximately every six weeks from March 2007 to January 2009. To avoid water and nutrient limitations, the plants were irrigated with water supplemented with nitrogen fertilizer using a surface drip irrigation system (Wall et al., 2011). Daily data sets on solar radiation, minimum and maximum canopy temperature, minimum and maximum air temperature at 2 m height, dew point, and wind speed at 2 m height are based on measurements from a weather station located in the experimental field and were supplemented with data from the AZMET weather station for times in which the on-site weather station was not available (Kimball et al., 2012). The HSC experiment also provides data for heated plots, where the plants were heated with IR heaters by additional 1.5°C in the day and 3°C in the night. However, in this work we only use the data from the control plots, i.e. which were not heated, as was done in Webber et al. (2017). For the analysis, we compute the RMSE_{so} between simulated and observed values (Eq. 14, Sect. 2.8), which was also used in Webber et al. (2017). Secondly, we use data from the China Wheat experiment. It was performed in 1985 and 1986 at five different locations in the North American Great Plains, namely Lethbridge (Alberta, Canada), Mandan (North Dakota, USA), Tryon (Nebraska, USA), Manhattan (Kansas, USA), and Lubbock (Texas, USA). Two cultivars of winter wheat were grown under four different nitrogen levels and three different irrigation regimes. However, we restrict our analysis to two water level regimes and only include experiments in which the crops were grown under limited (lowest) water availability and under well-irrigated conditions (highest water availability). Furthermore, we pool the results from experiments where two different intermediate nitrogen levels were applied, to harmonize the number of nitrogen levels with the three possible fertilizer application settings in LPJmL. We use canopy temperatures that were measured daily between noon and 4 pm local time with an infrared thermometer. Air temperature, humidity, wind speed, and radiation were measured at 2 m height every minute and were then aggregated to provide daily averages and/or totals, except for air temperature, where daily minimum and maximum values are reported. More details are provided in Reginato et al. (1988).

For the global evaluation of simulated mean and maximum canopy temperatures in LPJmL (Sect. 3.2.2), we use skin temperatures and 2 m air temperatures from ERA5 data. Skin temperatures represent the temperatures of the uppermost surface layer of the Earth, i.e. over land the vegetation layer, the top layer of bare soil, or the top layer of the snow pack. More information is given in Hersbach et al. (2018). ERA5 provides data starting only in the year 1940. To enable continuous LPJmL simulations from 1901 onwards (as needed for the spinup procedure, see Sect. 2.6), we use a processed dataset from ISIMIP. In this dataset, the years from 1901 to 1978 have been filled with daily GSWP3 data bias-adjusted to ERA5, using ISIMIP3BASD v2.5.1 (Kim, 2017; Hersbach et al., 2018; Lange et al., 2025). For the evaluation of simulated canopy temperatures, we select the year 1990. As in Drüke et al. (2021), we use skin temperatures as a proxy for canopy temperatures and assume they should be identical.

https://doi.org/10.5194/egusphere-2026-1898
Preprint. Discussion started: 18 May 2026

We first compare simulated canopy temperatures to ERA5 skin temperatures for cells with a land cover share of minimum 20% for rainfed wheat, and minimum 10% for all other crops, and with LAI values between 2 and 3.5 - 6.5 (depending on the crop specific maximum LAIs between 4 and 7) to catch the main growing season. Second, we analyze, whether skin temperatures in these cells are better represented by simulated canopy temperatures than by 2 m air temperatures. For this, we analyze the intercept, slope, coefficient of determination (R^2), and RMSE_{rp} (Sect. 2.8, Eq. 13) of a linear regression of simulated canopy temperatures or air temperatures, respectively, on skin temperatures. Furthermore, we compute the mean squared deviation (MSD), squared bias (SB), nonunity slope (NU), and a lack of correlation (LC) (see Sec. 2.8).

2.8 Evaluation metrics

For the analysis we mainly use nine metrics. Two of them are the intercept and slope of a linear regression, which give information about a potential offset and rotation of the regressor values relative to the values of the independent variable. We also analyze the coefficient of determination (R^2) as a third metric. Two more metrics both relate to the computation of the square root of the mean squared error (RMSE). One of the RMSEs is related to the linear regression, as follows

$$\mathrm{RMSE}_{rp} = \sqrt{\frac{1}{N}\sum_{i=1}^{N}(y_{r,i} - y_{p,i})^2}, \tag{13}$$

where $y_{r,i}$ is the ith value of the regressor (in this study emulated canopy temperatures) and $y_{p,i}$ the ith predicted value from the regression. The other RMSE relates simulated and observed data:

$$\mathrm{RMSE}_{so} = \sqrt{\frac{1}{N}\sum_{i=1}^{N}(y_{s,i} - y_{o,i})^2}, \tag{14}$$

where $y_{s,i}$ is the ith simulated and $y_{o,i}$ the ith observed value. RMSE_{rp} gives information about the performance of the linear regression, whereas RMSE_{so} provides insights into the differences or similarities between simulated and observed data.
Furthermore, we apply the metrics squared bias (SB), nonunity slope (NU), and lack of correlation (LC), which are measures for translation, rotation, and scatter between two data sets. The sum of these three metrics is the mean squared deviation (MSD), which can also be expressed as the sum of squared deviations between values on the x axis (i.e. skin temperatures in Sec. 3.2.2) and values on the y axis (i.e. simulated canopy temperatures or 2 m air temperatures, respectively, in Sec. 3.2.2), divided by the number of data points. It provides information on the equality between the two datasets. A more detailed explanation containing examples is provided by Gauch et al. (2003).

3 Evaluation

3.1 Performance of the emulators

The results of the cross validation of both mean and maximum emulators are shown in Fig. 1. The slopes of the linear fits are near one and intercepts are near zero for all cases, i.e. both for lower and upper canopy temperature limits and both temperature

https://doi.org/10.5194/egusphere-2026-1898
Preprint. Discussion started: 18 May 2026

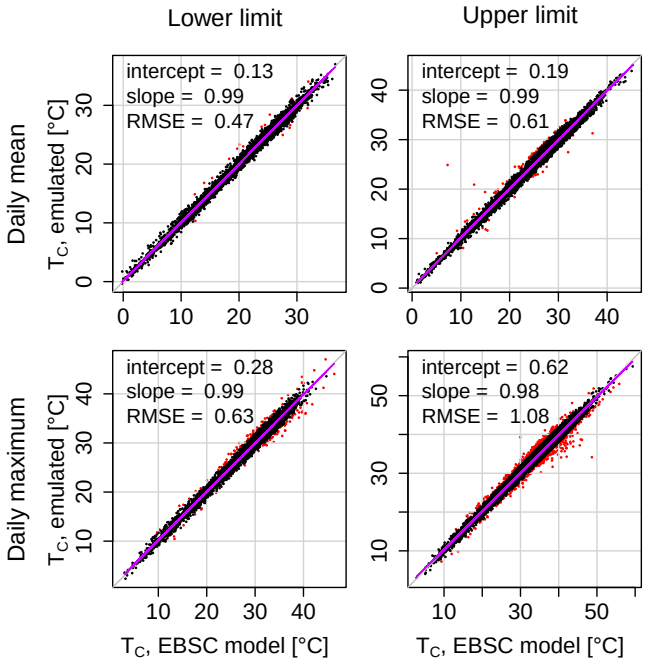

Figure 1. Comparison of canopy temperature outputs from the rebuilt EBSC model and the emulators for lower (first column) and upper (second column) limits. Plots in the first row represent daily mean values, plots in the second row daily maximum values. Red dots mark emulated canopy temperatures that differ more than 2 K from the EBSC results. Values for intercept, slope, and RMSE correspond to the respective linear fits (purple lines). The figure shows cross-validation results that have been produced with a validation input dataset which is independent from the training dataset.

ranges (daily mean and maximum values). Additionally, RMSEs are low for all limits (0.47 to 1.08 K). We conclude that, in general, the emulators represent the EBSC model results very well. Medium to large deviations, here defined as emulated results that differ more than 2 K from the EBSC model's results (see Fig. 1, red dots), are most pronounced for the upper canopy temperature limit of the maximum emulator, and are mainly caused by low wind speeds (Fig. 2). This seemingly weak point, however, reflects the emulator's capability to reproduce the characteristics of the EBSC model, which is prone to errors at low wind speeds (Webber et al., 2016).

3.2 Simulated canopy temperature in LPJmL

3.2.1 Site-specific comparison of simulated and observed differences between canopy and air temperatures

The developed emulators for lower and upper canopy temperature limits can easily be used in global models. We apply the innovative method in the global model LPJmL and show the results in this section. We test whether the emulators used in LPJmL provide meaningful results and compare the simulated final canopy temperatures with observed data. For this, we use

https://doi.org/10.5194/egusphere-2026-1898
Preprint. Discussion started: 18 May 2026

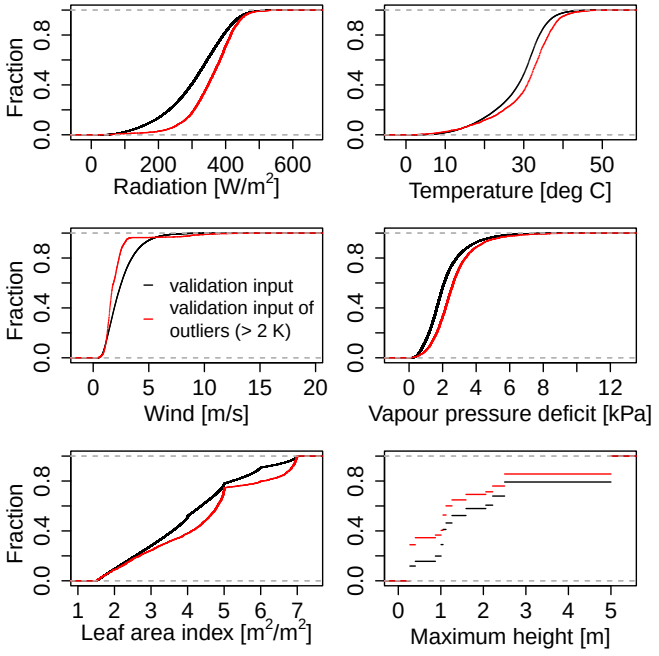

Figure 2. Cumulative density functions of the input variable values entering the upper canopy temperature limit emulator. Only input data for the cross-validation of daily maximum values are shown here. Black lines show input values of the full dataset, while red lines show only input values that lead to emulated canopy temperatures differing more than 2 K from EBSC results. Red lines correspond to red dots of the bottom-right subplot in Fig. 1. A steeper/flatter increase of the red lines compared to the black ones means that the corresponding variable value ranges lead to more/less errors in the emulated canopy temperature results.

canopy temperature data from two experiments and analyze the differences ΔT between canopy temperatures and near-surface air temperatures ($\Delta T = T_c - T_a$). Negative ΔT values represent cooling effects, i.e. the canopy temperature is lower than the
355 air temperature, while positive values represent heating effects.

1. Observational data from the HSC experiment The HSC experiment was conducted in Maricopa (Arizona, USA), where the climate is hot and arid. These quite specific conditions allow for a high water vapor pressure deficit, which allows the canopy to cool down when water stress is low. This effect can be seen in the observational data for irrigated wheat (Fig. 3). The simulated values generally reproduce this effect and are quite close to the observational data. However, the simulated
360 values show a bias towards overestimating ΔT. Qualitative deviations, where simulated canopy temperature differences show cooling effects while the observations show heating effects, are especially for cases where even observed canopy temperature measurements of replicates differ by up to 4.5 K (that have experienced almost the same treatment, with some deviations such as small differences in irrigation amounts).

2. Observational data from the China Wheat experiment In this section, we use data from the China Wheat experiment in
365 order to validate the approach's capacity to reproduce both cooling and heating effects. Figure 4 shows ΔT for different levels

https://doi.org/10.5194/egusphere-2026-1898
Preprint. Discussion started: 18 May 2026

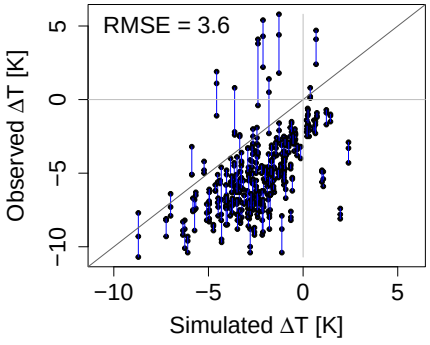

Figure 3. Comparison of simulated and observed differences ΔT between canopy temperatures and air temperatures ($\Delta T = T_c - T_a$) in Maricopa (Arizona, USA). Each black dot represents a measurement on a certain day for a specific plant. Blue lines show ranges of observed ΔT on a specific day for replicates that have experienced approximately the same treatment in the experiments. As replicates are treated equally in LPJmL, several observed ΔT values of replicas correspond to only one simulated value per day.

of nitrogen and water availability and different locations. In general, the extended LPJmL model is capable of reproducing both canopy temperatures that are higher and lower than near-surface air temperatures. When water is scarce and the nitrogen availability low (Fig. 4, top left plot), observations show mainly heating effects (66%, as opposed to 34% cooling effects). The heating effects are very well reproduced by the simulations, which is reflected by the very high rate of true positives (70%) and a low rate of false negatives (2%). The simulations hardly show any cooling effect and reproduce only 5% of the observed negative ΔT values. For higher nitrogen levels and rainfed conditions, observed heating effects are still well captured by the simulations (true positives with relatives rates of 65% and 66%). For high nitrogen and high water availability (Fig. 4, third row, right-hand plot), cooling effects dominate over heating effects in the observations (76% over 24%). These dominating effects are reproduced by LPJmL with a true negative rate of 55%. For a medium nitrogen level and a high water level (plot in the right-hand column of the second row), simulated ΔT values show mainly heating effects while observations have a clear tendency towards cooling effects. However, the observed ΔT values of experimental replicates here also span wide ranges, of which some even stretch from positive to negative ΔTs.

3.2.2 Global assessment of simulated canopy temperatures

In order to analyze the applicability of the emulator approach in LPJmL at the global scale, we compare simulated canopy temperatures to a global dataset of ERA5 skin temperatures, which reflect the Earth's topmost surface layer (as described in Sec. 2.7). Furthermore, we examine whether simulated canopy temperatures reproduce the skin temperatures more accurately than the 2 m air temperatures do, to evaluate whether the net benefit of employing simulated canopy temperatures outperforms the established use of the standard air temperatures.

The simulated wheat canopy temperatures in LPJmL (T_c) show a greater variation than the ERA5 2 m air temperatures (T_a) when compared to ERA5 skin temperatures (Skt) (Fig. 5). For daily mean temperatures (Fig. 5, first row), T_c overestimates

https://doi.org/10.5194/egusphere-2026-1898
Preprint. Discussion started: 18 May 2026

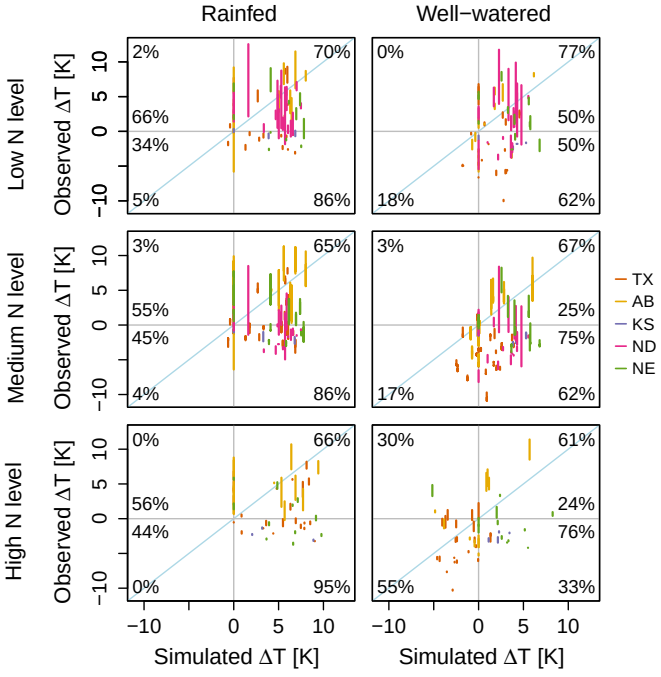

Figure 4. Comparison of simulated and observed differences ΔT between canopy temperatures and air temperatures ($\Delta T = T_c - T_a$) at five different locations (Lubbock, Texas (TX); Lethbridge, Alberta (AB); Manhattan, Kansas (KS); Mandan, North Dakota (ND); Tryon, Nebraska (NE)) and for different levels of nitrogen and water availability. Negative values indicate cooling effects of the canopy, whereas positive values show heating effects. Vertical lines represent ranges of observed replicates' values at a specific day and location, respectively. For replicates, the same simulation settings are used in LPJmL. Thus, several observed ΔT values of replicas correspond to only one simulated value. Grey lines divide the plots into four qualitative parts, where the top right and the bottom left quarters indicate true positives and true negatives, i.e. simulated ΔT values that reproduce the heating and cooling effects of the observations. Top left and bottom right quarters include false negatives and false positives. Numbers in the corners indicate the share of heating/cooling effects, that have (top right/bottom left) or have not (top left/bottom right) been reproduced by the simulations in percent. The numbers indicating these shares in the upper or lower half, respectively, do not sum up to 100% as some simulated ΔT values equal zero. Numbers above and below the zero line show the relative amounts of observed positive and negative ΔT values in percent.

Skt, while T_a overestimates Skt at lower but underestimates it at higher temperatures. Both slopes are around one, however, canopy temperatures show a stronger bias compared to air temperatures due to a greater positive shift. When looking at daily maximum skin temperatures (Fig. 5, second row), T_a clearly underestimates Skt with an increasing bias for rising temperatures, while T_c matches Skt quite well with only a very small positive, constant bias. This means that, especially for high temperatures
390 that are important for heat stress related processes, T_c represents Skt values well whereas T_a significantly underestimates Skt . These results are also reflected in the components of the mean squared differences, which can be partitioned into a lack of correlation (LC), a mean squared bias (SB), and a nonunity slope (NU). LC, which is associated with the spread between Skt and T_c or T_a, is higher for daily maximum temperatures than for daily mean temperatures and higher for T_c than for T_a for all

https://doi.org/10.5194/egusphere-2026-1898
Preprint. Discussion started: 18 May 2026

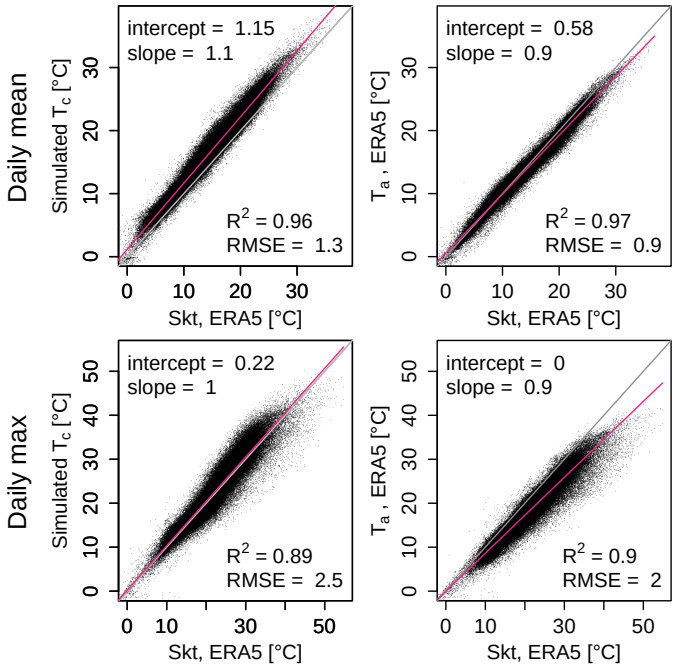

Figure 5. Comparison of simulated wheat canopy temperatures computed in LPJmL (T_c, first column) and ERA5 2 m air temperatures (T_a, second column) to ERA5 skin temperatures (Skt), respectively. Both daily mean (first row) and daily maximum (second row) temperatures are shown. Each dot refers to one day and cell of a global grid, where rainfed wheat has a share of minimum 20%. Simulated canopy temperatures correspond to rainfed wheat only, whereas ERA5 skin temperatures are based on the total surface area of the respective cells.

crops except for cassava and field pea (Fig. 6 and Fig. B2 - B4). Daily mean T_a shows a smaller MSD than daily mean wheat T_c, mainly due to the substantially smaller squared bias. T_c MSDs, and their relation to T_a MSDs, of soybean, rice, rapeseed, and groundnut is approximately similar, while the MSD of groundnut T_c is a bit higher compared to the other crops. For the remaining crops, i.e. maize, sugarcane, sugar beet, cassava, millet, sunflower, and field pea, the differences in MSDs of T_a and T_c are not as clear cut and both perform very well (Fig. B2, B3, B4). When looking at daily maximum values, T_c performs significantly better than T_a, which applies to all crops tested in this study. This is mainly due to the comparatively very small SBs, but also because of very small NU values.

4 Discussion and conclusions

In this study, we describe a novel approach to compute canopy temperatures of crops, whose low computational costs makes it suitable for use in global, computationally expensive models. For this, we provide canopy temperature emulators that are based on a complex energy-balance approach correcting for atmospheric stability conditions and validated in LPJmL. The emulators are applicable to a wide range of weather conditions, as they are trained on a large dataset including historic and future

https://doi.org/10.5194/egusphere-2026-1898
Preprint. Discussion started: 18 May 2026

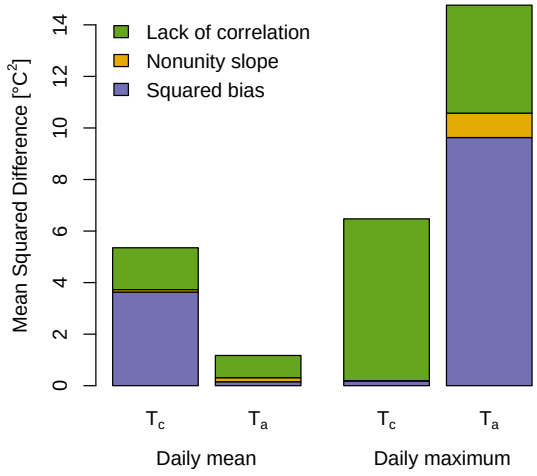

Figure 6. Mean squared differences between ERA5 skin temperatures and simulated canopy temperatures (T_c) or ERA5 2 m temperatures (T_a) for daily mean and daily maximum values.

conditions. However, when used with data outside or at the borders of the training range, the emulators should be used very cautiously as they can easily produce artifacts. We therefore recommend that the global models using the emulators incorporate thresholds for different variables that restrict canopy temperatures once the limits are exceeded, following the methodology applied in this study.

We show, for wheat, that the emulator approach in LPJmL can reproduce both observed heating and observed cooling effects and that the simulated canopy temperature dynamically responds to the water and nitrogen status of a crop. However, there are deviations between simulated canopy temperatures and observed values for all experimental sites, which can have different potential causes. First, observed and simulated canopy temperatures potentially relate to, at least partially, different climatic conditions, resulting from the temperature and radiation related assumptions made in this study. While we think that the coincidence of daily maximum air and daily maximum canopy temperature at 3 pm and a sinusoidal radiation curve are valid approximations in global scale applications, the error they cause might be exposed in comparison to case-specific observations. Second, the growth and development of crops in LPJmL very probably differs from the observations, which can have significant effects on LAI and water stress. We reduce the error by using sowing date inputs and information on maturity from both experiments. In the HSC simulations, we achieve an even greater reduction by combining these dates with a calibration of LAI, which was however not possible in the China Wheat simulations due to a lack of data. Third, in LPJmL simulations, we use a combination of various configuration settings and global inputs that together are intended to represent a specific agricultural management system. One of the tunable settings of this management, for example, would be the level of nitrogen

https://doi.org/10.5194/egusphere-2026-1898
Preprint. Discussion started: 18 May 2026

availability. As we do not use the exact management related data from the experiments, such as the amount of fertilizer applied, the simulated growing conditions deviate from the experimental conditions, to a lesser or greater extent depending on the specific setting and input. We decided for this option to evaluate whether LPJmL can qualitatively reproduce the results within its setting options. Lastly, Webber et al. (2025) show a systematic bias towards underestimation of simulated water use by analyzing several crop models that simulate daily evapotranspiration (ET) based on different approaches. The study finds that this bias is particularly pronounced under well-watered conditions. Though the LPJmL model was not part of the study of Webber et al. (2025), these findings could also apply here as LPJmL simulates ET based on reference crop estimates, as some of the evaluated models do, which causes errors in ΔT.

Variabilities between simulations and observations have also been reported in a comparison study by Webber et al. (2017), which compares different approaches to compute wheat canopy temperatures in different models. They show that in total, i.e. for the combined model results per approach, the EBSC approaches perform best, followed by empirical approaches and simple energy balance approaches. Comparing the RMSEs between simulated and observed canopy temperatures in Maricopa of LPJmL (RMSE = 3.6) and the models using EBSC approaches presented in Webber et al. (2017) (RMSE = 1.4-4.4) reveals that the performance of LPJmL ranks between the three EBSC models. It performs worse compared to the two models that use the EBSC approach on which the emulators are based on. This is not surprising, as an emulator cannot outperform its parent model. However, LPJmL performs substantially better than a different EBSC-model-combination and performs significantly better than all EBN models evaluated in the comparison study. It is important to reiterate that the comparison concerns the combination of methodology and model and that it is not the results of the different canopy temperature approaches themselves. For example, the definition and computation of water stress in LPJmL has an impact on the results of the simulated canopy temperatures. Our results therefore show that the synergy between our developed emulator approach and LPJmL performs well compared to the previously analyzed approaches embedded in the corresponding crop models.

Executing the further developed LPJmL model globally for 100 years and with a spatial resolution of 0.5° requires additional compute time of approximately 3% compared to a baseline simulation, where only near-surface air temperatures are used. Thus, with the emulator approach, canopy temperatures can now be computed and used in LPJmL without significantly increasing the runtime. For the scaling between upper and lower canopy temperature limit to compute final canopy temperatures, we use a water stress factor that uses the relation between the actual canopy conductance computed in LPJmL and the theoretical optimal canopy conductance for a specific LAI. We consider this type of scaling most consistent with the original EBSC approach. Other water stress factors, such as one that relates actual and potential transpiration, might also be applicable.

For the global-scale evaluation, we compute mean squared deviations (MSDs) for simulated canopy temperatures and ERA5 2 m air temperatures, both compared to ERA5 skin temperatures. For simulated wheat canopy temperatures, the lack of correlation (LC) is higher than for 2 m air temperatures, both for daily mean and daily maximum values. This also applies to most of the other crops examined in this study. We included LC for completeness, however, we think that it is not a relevant metric to evaluate the skill of LPJmL to globally simulate canopy temperatures. This is because we have limited ability to harmonize the underlying assumptions between ERA5 and LPJmL simulations, due to a lack of information. This particularly concerns the vegetation structure and status ERA5 data is based on, such as the distribution of natural vegetation, land-use patterns, and the

https://doi.org/10.5194/egusphere-2026-1898
Preprint. Discussion started: 18 May 2026

canopy status of a crop, especially with regard to LAI and water stress. As these matter for the canopy temperatures and may all mismatch to some extent, we don't expect that we can exactly reproduce the variation of skin temperatures. The NUs for daily mean ERA5 air temperatures and simulated wheat canopy temperatures are both very small. However as the SB is significantly smaller for T_a compared to T_c, daily mean ERA5 air temperatures perform better compared to daily mean canopy temperatures. From this, we conclude that, for wheat, daily mean 2 m air temperatures are a better approximation for daily mean skin temperatures. The same applies to soybean, rice, rapeseed, and groundnut. For the other crops, T_a performs only slightly better and the MSDs of both T_a and T_c are relatively small. This outcome confirms that using daily mean air temperatures to derive the water stress factor needed for the computation of the canopy temperature is a valid simplification we apply in LPJmL. It also indicates that when simulating canopy temperatures on a daily timestep and with a spatial resolution of 0.5°, sticking with 2 m air temperature inputs in processes that are driven by mean temperatures might be a better choice. In contrast, for all crops, daily maximum canopy temperatures significantly better reproduce maximum skin temperatures compared to daily maximum air temperatures, which we think is a clear improvement. This becomes especially pronounced at high temperatures, due to the comparatively small non-unity slope and the very large improvement in the squared bias compared to the respective MSD components of the air temperature.

Overall, the developed emulators provide a robust and lightweight option to compute canopy temperatures in global crop models. This allows the incorporation of actual canopy temperatures into temperature-dependent processes, particularly those related to heat stress, in large-scale crop model applications. This constitutes a solid basis for better simulating the impacts of high temperatures on crop growth and yield. Considering actual daily maximum canopy temperatures instead of near-surface air temperatures can help to avoid underestimating climate impacts, especially under drought conditions.

Code and data availability. The source code of the rebuilt EBSC model, the emulators, and LPJmL as described in this study is available at https://doi.org/10.5281/zenodo.18937839 (Hemmen et al., 2026) and is licensed under the GNU Affero General Public License v3.0 or later. The maximum crop height data was compiled from National Plant Germplasm System, United States Department of Agriculture-Agricultural Research Service (2025) and Byrne et al. (2018). The respective accession numbers are provided in the Supplement. The climate data from the ISIMIP3b data set are available from https://data.isimip.org/10.48364/ISIMIP.842396.1 (Lange and Büchner, 2021).

https://doi.org/10.5194/egusphere-2026-1898
Preprint. Discussion started: 18 May 2026

Appendix A: Parameter values and variable units

Table A1. Maximum heights of different crops used as input in the EBSC model and the emulators. Sources of crops marked with * are National Plant Germplasm System, United States Department of Agriculture-Agricultural Research Service (2025) and Byrne et al. (2018).

Crop	**Maximum height**	**Source**
Cassava	2.5 m	Pongsivapai et al. (2016)
Groundnut	0.4 m	Lieberei et al. (2007)
Sugarcane	5 m	Lieberei et al. (2007)
Maize	2.2 m	*
Millet	1.6 m	*
Pea	1.0 m	*
Rapeseed (*Brassica*)	1.3 m	*
Rice	1.1 m	*
Soybean	0.9 m	*
Sugarbeet	0.3 m	*
Sunflower	2.1 m	*
Wheat	1.1 m	*

Table A2. Units and conditions of the variables used in the ordinary least squares fit and therewith corresponding to the derived parameter values listed in Table A3 and Table A4.

Input variable	Unit	Condition
canopy temperature limit	°C	
radiation	W/m^2	net radiation
near-surface air temperature	°C	at 2 m height
wind speed	m/s	at 10 m height
vapour pressure deficit	kPa	
leaf area index	m^2/m^2	
maximum height	m	at maturity

https://doi.org/10.5194/egusphere-2026-1898
Preprint. Discussion started: 18 May 2026

Table A3. Parameter values of the emulator representing the daily mean / daily maximum lower canopy temperature limit.

Term	Corresponding parameter value (mean / maximum)	Term	Corresponding parameter value (mean / maximum)
Intercept	0.684738629964106 / 0.335499806107242	LAI · T^2	7.02513304605671e-05 / 3.02818676194859e-05
R	0.0238257241845737 / 0.0177118632192518	H · T^2	-8.52108910466774e-05 / 4.91111517515602e-06
T	0.979442593610725 / 1.13363321594806	R · W^2	-0.000370985873459898 / -0.000196398310315102
W	0.424136320631572 / 0.885945332166679	T · W^2	-0.00124707201166279 / 0.0053432713082662
VPD	-1.98165531732936 / -2.5295482937045	VPD · W^2	0.108561714526047 / 0.0219786139240005
LAI	-0.464528073458259 / -1.00751368780178	LAI · W^2	-0.00132870062225791 / 0.00375486500339963
H	-0.754608160742413 / -0.54279847889252	H · W^2	0.00520401914828577 / -0.000300448260456604
R^2	-9.44061068285206e-05 / -4.59459188249794e-05	R · VPD^2	0.0010330439796772 / 0.000167319141876229
T^2	-0.00174754820852831 / -0.00734879684534497	T · VPD^2	0.0108324713718574 / 0.0188273223906645
W^2	-0.070825455126643 / -0.0720252139007607	W · VPD^2	-0.0156377861877198 / -0.0503351790124593
VPD^2	-0.393446083839767 / -0.373666664716829	LAI · VPD^2	-0.000687292903273528 / 0.013019580317415
LAI^2	0.152415964418906 / 0.337190557092204	H · VPD^2	0.0272852478093777 / 0.018202920435506
H^2	0.273190377993691 / 0.218964285660971	R · LAI^2	7.736095495361e-05 / 6.15635728409753e-05
R^3	9.07247563839932e-08 / 1.19256789787197e-08	T · LAI^2	-0.00116383357003676 / 0.000300955415487673
T^3	6.47691040505406e-05 / 0.000153084241073099	W · LAI^2	0.0162250907310742 / 0.019386376778815
W^3	0.00432101840215569 / -0.00031482838499385	VPD · LAI^2	0.0658622040335229 / 0.0385435799754048
VPD^3	-0.0169096986037111 / -0.0267441593955635	H · LAI^2	-0.00587867646765619 / -0.0045796577422814
LAI^3	-0.0129652948888963 / -0.0276418924345715	R · H^2	0.000362059507275255 / 0.000223699910849714
H^3	-0.0292182378046877 / -0.0235347650377727	T · H^2	-0.000867245645110482 / -0.000973807025638765
R · T	-2.49802501549612e-05 / 0.000328843493408458	W · H^2	-0.00831032582577907 / -0.00246722167298038
R · W	0.0021334007280068 / 0.00253216041699921	VPD · H^2	-0.0412102307472056 / -0.0231204288210232
T · W	0.0111424266140398 / -0.0360284007746833	LAI · H^2	0.00213455714194835 / 0.00185054253433549
R · VPD	0.00852333254844296 / 0.00358640063253502	R · T · W	-6.87164907853102e-05 / -0.000152203404572209
T · VPD	0.0813163320277646 / 0.0995783203701648	R · T · VPD	-7.8804795094112e-05 / -0.000104971941843597
W · VPD	-0.665901941095188 / -0.477377144592702	R · W · VPD	-0.00078504405395761 / 0.000362252313838042
R · LAI	0.000100224568748763 / -0.000422370499479933	T · W · VPD	0.00694589065001527 / 0.0161995426769113
T · LAI	0.00188998392274073 / -0.0091973061844597	R · T · LAI	-3.05884116244213e-05 / 8.8092037991244e-06
W · LAI	-0.127036901741507 / -0.21901853162744	R · W · LAI	0.000184224764567332 / 0.00011162215897887
VPD · LAI	-0.674830377465252 / -0.344698645458475	T · W · LAI	0.000897678488249315 / -0.000708874055023871
R · H	-0.00410005727344349 / -0.00282308361531423	R · VPD · LAI	0.000317118218215186 / -0.000201759716701147
T · H	0.0021682139371747 / 0.00392328191307234	T · VPD · LAI	0.00982136124671707 / 0.00357499736331164
W · H	0.0597937304639833 / 0.0386377300967347	W · VPD · LAI	-0.0916799884652602 / -0.0489669806978538
VPD · H	0.4567970683386 / 0.255384078068201	R · T · H	6.9495725761049e-05 / 3.57510407303981e-05
LAI · H	0.0166280132921359 / -0.0267510563926032	R · W · H	-3.05955023393419e-05 / -7.17374317926158e-05
T · R^2	2.58410909677867e-06 / 8.73211648132386e-07	T · W · H	-0.000773610419593476 / -0.00115810137527362
W · R^2	7.92674275800157e-06 / 3.02624895560436e-06	R · VPD · H	-0.000181278868313015 / -0.000191522508760132
VPD · R^2	-2.47380225994339e-05 / -2.13771687466589e-06	T · VPD · H	-0.00503912440544421 / -0.00458532950408962
LAI · R^2	-2.12176392679634e-06 / 3.35708188275551e-08	W · VPD · H	0.00457508606831037 / 0.0297275271507688
H · R^2	-6.14975941182877e-07 / 9.82799882271981e-07	R · LAI · H	-3.2032802401298e-05 / -3.66696712298234e-05
R · T^2	-1.24460569447719e-05 / 6.16392329277969e-06	T · LAI · H	0.00158092912469135 / 0.00162244615085394
W · T^2	-8.14178109201921e-07 / 0.000248595705594688	W · LAI · H	-0.0053144780767882 / 0.00331012001955864
VPD · T^2	-0.00156075338890622 / -0.00260224547239092	VPD · LAI · H	-0.0212962135011556 / -0.0171504739425066

https://doi.org/10.5194/egusphere-2026-1898
Preprint. Discussion started: 18 May 2026

Table A4. Parameter values of the emulator representing the daily mean / daily maximum upper canopy temperature limit.

Term	Corresponding parameter value (mean / maximum)	Term	Corresponding parameter value (mean / maximum)
Intercept	1.57294631444757 / 1.19294101105091	LAI · R^2	-4.8041733996011e-06 / -2.42835751070472e-06
R	0.0215907803831365 / 0.00547724925045655	H · R^2	3.18331295385831e-06 / 2.25339210134643e-06
T	0.959197030517232 / 0.996899566609795	R · T^2	-5.56236232454854e-06 / -1.26162095997905e-06
W	0.646165184710429 / 2.02531928613433	W · T^2	-0.000211286604898744 / 0.000334474059186617
LAI	-0.850956452607541 / -1.11525704338414	LAI · T^2	-3.97785272027009e-05 / -0.000139229749596059
H	-1.6891060886083 / -2.15805534174577	H · T^2	-0.000119226034280661 / -0.000259398851172051
R^2	-7.63633065147557e-05 / -2.52738596950725e-05	R · W^2	-0.000680742358364853 / -0.000592367548017471
T^2	0.000198008049330144 / 0.000552687105730965	T · W^2	-0.00302706128362604 / 0.000132379565485438
W^2	-0.19508448928111 / -0.407553848908752	LAI · W^2	-0.0360698543145224 / -0.0407024107089903
LAI^2	0.221504574058072 / 0.295346035616088	H · W^2	0.0281158944365907 / 0.0705829796694067
H^2	0.940296845415715 / 1.4971921077902	R · LAI^2	-0.000239291383930677 / -0.000225996115685937
R^3	5.09077630190997e-08 / 1.58210592791247e-08	T · LAI^2	0.000776693178493996 / 0.00157276531513076
T^3	2.23464226281022e-05 / -1.08516930914652e-05	W · LAI^2	0.0419982079957769 / 0.0610309983889868
W^3	0.0203162526973146 / 0.027653486908925	H · LAI^2	-0.00329631005508651 / -0.00699056254750224
LAI^3	-0.0220806046954664 / -0.0319303841246007	R · H^2	0.00108516622495528 / 0.000662350780325776
H^3	-0.126934427374181 / -0.216622965417301	T · H^2	0.000440370193117213 / 0.00169853872632537
R · T	2.07414789606958e-05 / 0.000120278218954617	W · H^2	-0.0124497325684132 / 0.0287972793787918
R · W	0.00275490700320539 / 0.0061652854251486	LAI · H^2	0.0173574767443609 / 0.0210689719519521
T · W	0.0268809018783207 / -0.00916518268479086	R · T · W	2.64382061397449e-06 / -4.35948243795216e-05
R · LAI	0.00167531664304276 / 0.00109911381750646	R · T · LAI	6.42044087367724e-06 / 3.52774815366676e-05
T · LAI	-0.00213911087413184 / -0.0025611838700471	R · W · LAI	0.000807437320911396 / 0.000556238267869921
W · LAI	-0.0375028992555271 / -0.0785804320839716	T · W · LAI	-0.000256931648483477 / -0.00168750248054969
R · H	-0.00812126429013598 / -0.0037662266098979	R · T · H	2.27898533986115e-05 / -4.89970654807385e-06
T · H	-0.000301915081884917 / 0.00157500078419495	R · W · H	-0.000504784031825883 / -0.000789791225985831
W · H	-0.00994163372943662 / -0.58461292898057	T · W · H	0.000661445613035769 / 0.00365446383607496
LAI · H	-0.0384936426414885 / 0.016059049354213	R · LAI · H	4.02992821059829e-05 / 4.07303409202784e-05
T · R^2	7.25198506959094e-07 / 4.32197814310046e-08	T · LAI · H	-0.00039853702700531 / -0.00206459434696308
W · R^2	1.02219334698971e-05 / 1.77370782650859e-06	W · LAI · H	-0.0251277275969917 / -0.0267663544999401

https://doi.org/10.5194/egusphere-2026-1898
Preprint. Discussion started: 18 May 2026

Appendix B: Additional figures

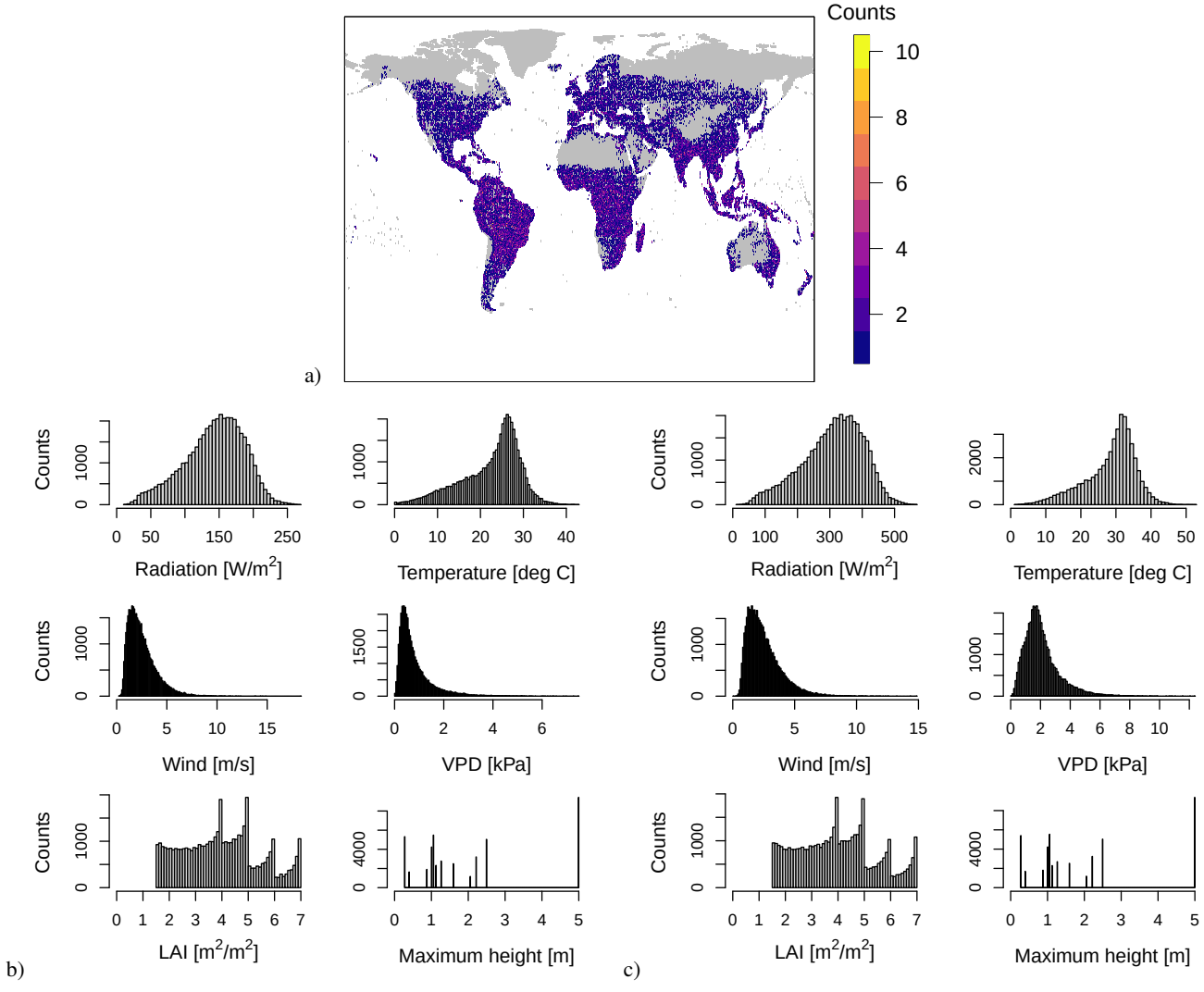

Figure B1. Selected cells (a) and corresponding variable values (b, c) used to drive the EBSC model and to train the emulators. The selection of cell-day cases was done as described in Sec. 2.2. Colors indicate how many times a cell appears in the assembled global input dataset, whereas gray colors show cells that are not considered. The histograms show spatially averaged cell-day values of the training dataset used to receive daily mean (b) and daily maximum canopy temperature limits (c).

https://doi.org/10.5194/egusphere-2026-1898
Preprint. Discussion started: 18 May 2026

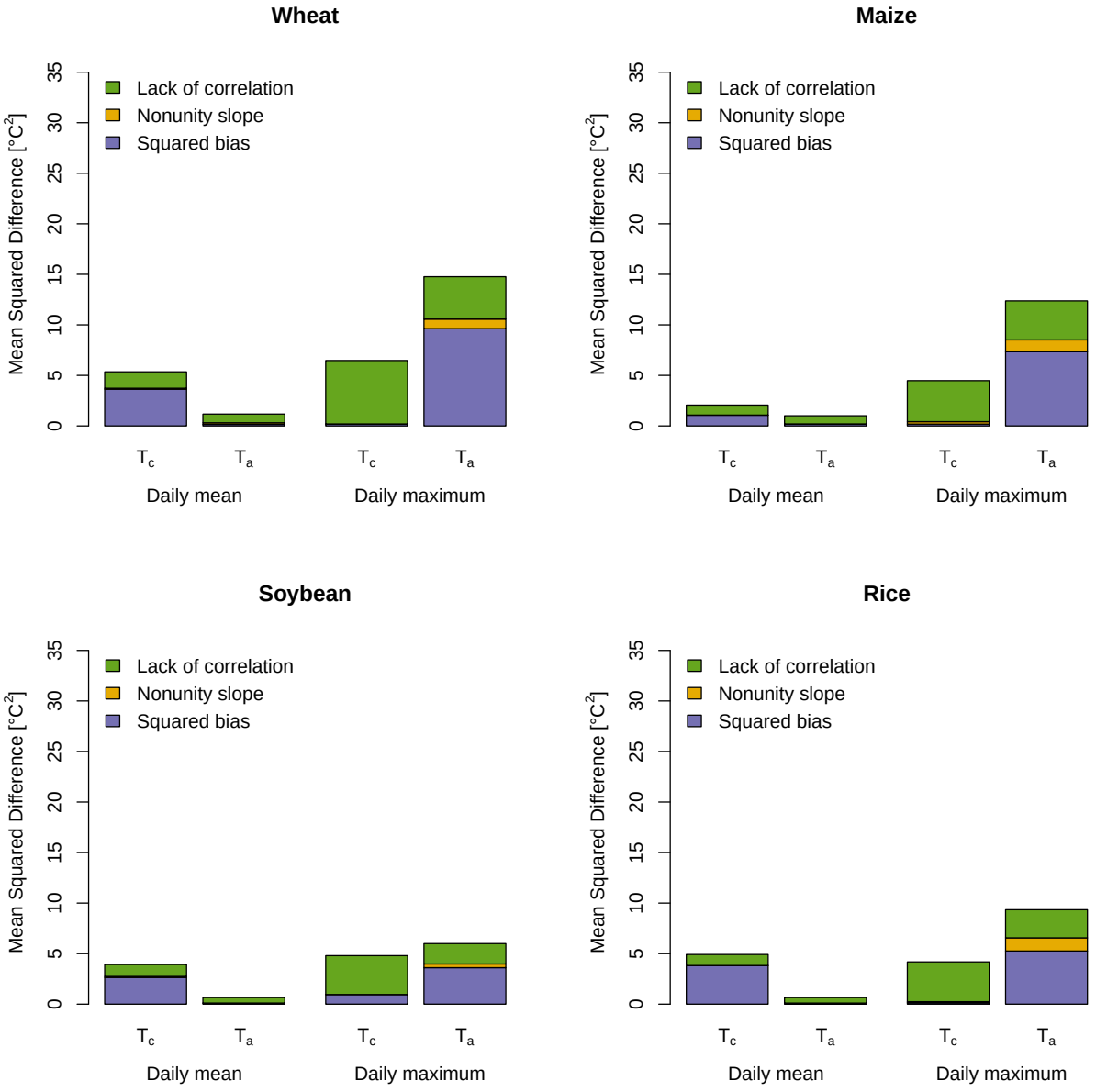

Figure B2. Same figure as Fig. 6, but for wheat, maize, soybean, and rice.

https://doi.org/10.5194/egusphere-2026-1898
Preprint. Discussion started: 18 May 2026

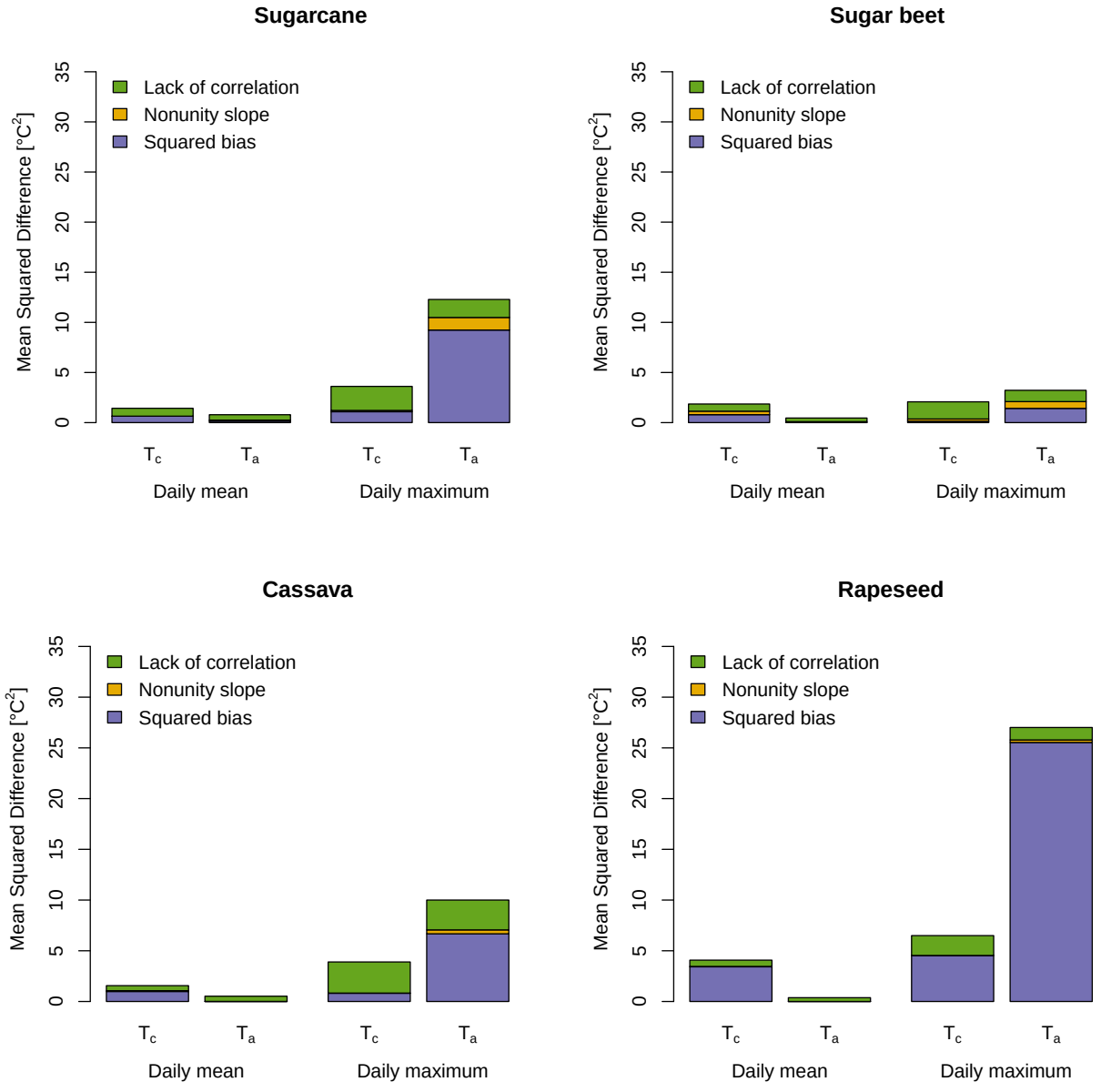

Figure B3. Same figure as Fig. 6, but for sugarcane, sugar beet, cassava, and rapeseed.

https://doi.org/10.5194/egusphere-2026-1898
Preprint. Discussion started: 18 May 2026

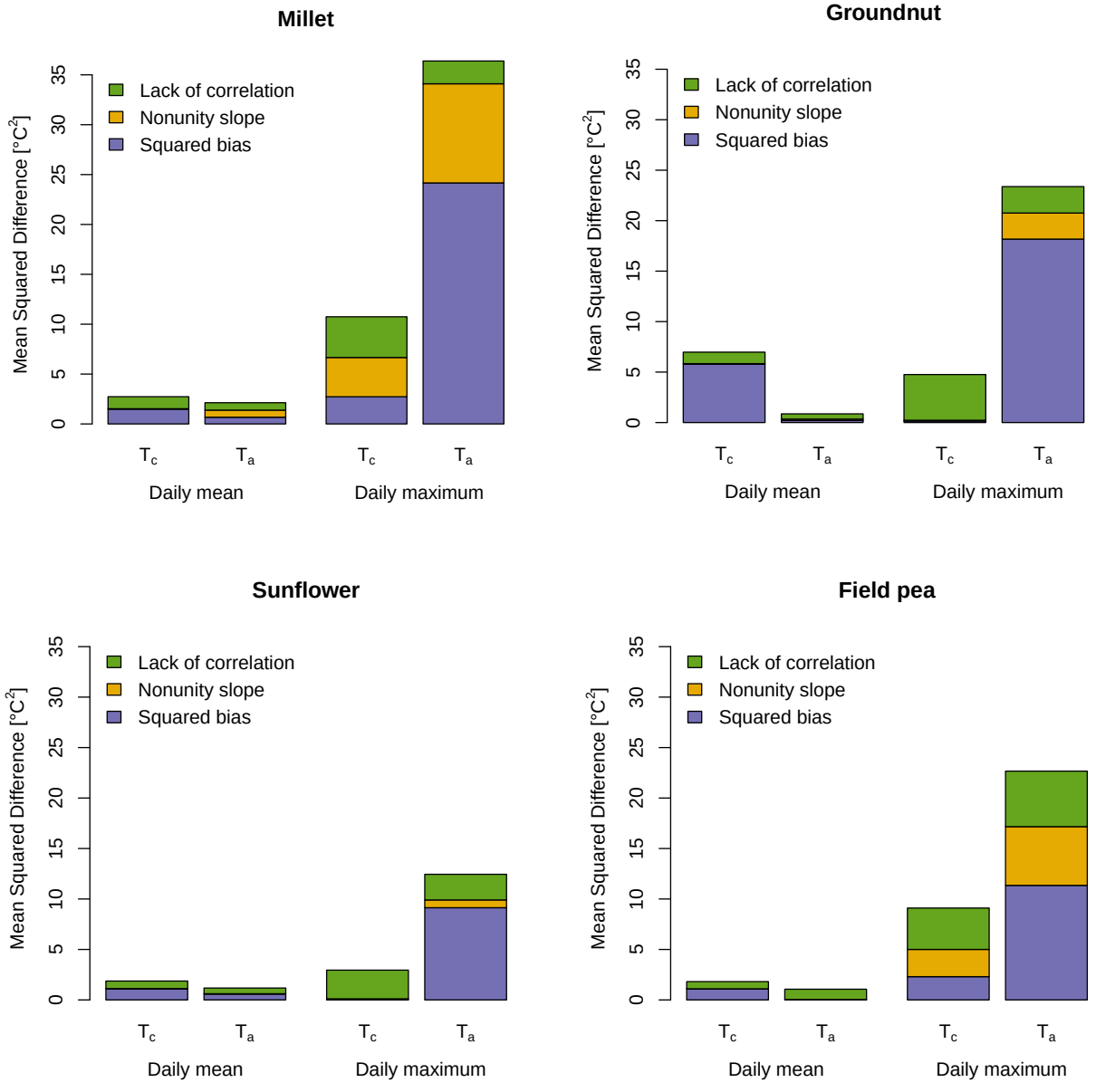

Figure B4. Same figure as Fig. 6, but for millet, groundnut, sunflower, and field pea.

https://doi.org/10.5194/egusphere-2026-1898
Preprint. Discussion started: 18 May 2026

Author contributions. MH and CM conceptualized and designed the study. MH rebuilt the EBSC model based on a model from and in exchange with HW. MH developed the emulators. MH and WvB conducted the implementation in LPJmL. MH, CM, WvB, and JH worked on the general LPJmL model maintenance and development. MH performed the model simulations and analyzed and visualized the results. MH wrote the original draft, which was reviewed and edited by MH, CM, and HW. All authors discussed the simulation results and analysis steps and reviewed and edited the manuscript.

Competing interests. At least one of the (co-)authors is a member of the editorial board of *Geoscientific Model Development*.

Acknowledgements. MH is funded by the German Federal Environment Foundation (Deutsche Bundesstiftung Umwelt, DBU), under the Grant AZ20021/707. She has also received funding from the German Federal Ministry of Research, Technology and Space through the ABCDR project (FKZ 01LS2105A). HW acknowledges funding from the Leibniz Association Female Professorship (award number P102/2020) and the German Research Foundation, (DFG Project Number: 470400637). JH has received funding from the European Union through the ClimTip project (project number 101137601) and from the Future of Life Institute through the CODEC project. We would like to thank Dr. Stefan Lange for the processing of ISIMIP data, especially the GSWP3-ERA5 data. Hersbach et al. (2018) was downloaded from the Copernicus Climate Change Service (2023) (Copernicus Climate Change Service (C3S) Climate Data Store (CDS), 2023). The results contain modified Copernicus Climate Change Service information 2020. Neither the European Commission nor ECMWF is responsible for any use that may be made of the Copernicus information or data it contains. The authors gratefully acknowledge the European Regional Development Fund (ERDF), the German Federal Ministry of Education and Research and the Land Brandenburg for supporting this project by providing resources on the high performance computer system at the Potsdam Institute for Climate Impact Research. The authors used large language models, such as ChatGPT, for text improvement. Subsequently, the authors reviewed and edited the content and they take full responsibility for the content of the published work.

https://doi.org/10.5194/egusphere-2026-1898
Preprint. Discussion started: 18 May 2026

References

Allen, R. G. and Wright, J. L.: Translating wind measurements from weather stations to agricultural crops, Journal of Hydrologic Engineering, 2, 26–35, 1997.

Amani, I., Fischer, R., and Reynolds, M.: Canopy temperature depression association with yield of irrigated spring wheat cultivars in a hot climate, Journal of Agronomy and Crop Science, 176, 119–129, 1996.

Asseng, S., Ewert, F., Martre, P., Rötter, R. P., Lobell, D. B., Cammarano, D., Kimball, B. A., Ottman, M. J., Wall, G. W., White, J. W., et al.: Rising temperatures reduce global wheat production, Nature climate change, 5, 143–147, 2015.

Breier, J., Ostberg, S., Wirth, S. B., Hötten, D., Minoli, S., Stenzel, F., and Müller, C.: lpjmlkit: A toolkit for operating LPJmL and model-specific data processing, Journal of Open Source Software, 9, 5447, 2024.

Byrne, P. F., Volk, G. M., Gardner, C., Gore, M. A., Simon, P. W., and Smith, S.: Sustaining the future of plant breeding: The critical role of the USDA-ARS National Plant Germplasm System, Crop Science, 58, 451–468, 2018.

Büchner, M. and Reyer, C.: ISIMIP3b atmospheric composition input data (v1.1), ISIMIP Repository [data set], https://doi.org/https://doi.org/10.48364/ISIMIP.482153.1, 2022.

Chambers, J. M.: Linear models, in: Statistical Models in S, edited by Chambers, J. M. and Hastie, T. J., chap. 4, Wadsworth & Brooks/Cole, 1992.

Clawson, K., Jackson, R., and Pinter Jr, P. J.: Evaluating plant water stress with canopy temperature differences, Agronomy Journal, 81, 858–863, 1989.

Copernicus Climate Change Service (C3S) Climate Data Store (CDS): Copernicus Climate Change Service (2023): ERA5 hourly data on single levels from 1940 to present, (accessed on April 2025), https://doi.org/10.24381/cds.adbb2d47, 2023.

Coumou, D. and Rahmstorf, S.: A decade of weather extremes, Nature climate change, 2, 491–496, 2012.

Drüke, M., von Bloh, W., Petri, S., Sakschewski, B., Schaphoff, S., Forkel, M., Huiskamp, W., Feulner, G., and Thonicke, K.: CM2Mc-LPJmL v1. 0: biophysical coupling of a process-based dynamic vegetation model with managed land to a general circulation model, Geoscientific Model Development Discussions, 2021, 1–33, 2021.

Enders, A., Vianna, M., Gaiser, T., Krauss, G., Webber, H., Srivastava, A. K., Seidel, S. J., Tewes, A., Rezaei, E. E., and Ewert, F.: SIMPLACE—a versatile modelling and simulation framework for sustainable crops and agroecosystems, in silico Plants, 5, 2023.

Franke, J. A., Müller, C., Elliott, J., Ruane, A. C., Jägermeyr, J., Snyder, A., Dury, M., Falloon, P. D., Folberth, C., François, L., et al.: The GGCMI Phase 2 emulators: global gridded crop model responses to changes in CO 2, temperature, water, and nitrogen (version 1.0), Geoscientific Model Development, 13, 3995–4018, 2020.

Friedlingstein, P., O'Sullivan, M., Jones, M. W., Andrew, R. M., Bakker, D. C. E., Hauck, J., Landschützer, P., Le Quéré, C., Luijkx, I. T., Peters, G. P., Peters, W., Pongratz, J., Schwingshackl, C., Sitch, S., Canadell, J. G., Ciais, P.and Jackson, R. B., Alin, S. R., Anthoni, P., Barbero, L., Bates, N. R., Becker, M., Bellouin, N., Decharme, B., Bopp, L., Brasika, I. B. M., Cadule, P., Chamberlain, M. A., Chandra, N., Chau, T.-T.-T., Chevallier, F., Chini, L. P., Cronin, M., Dou, X., Enyo, K., Evans, W., Falk, S., Feely, R. A., Feng, L., Ford, D. J., Gasser, T., Ghattas, J., Gkritzalis, T., Grassi, G., Gregor, L., Gruber, N., Gürses, , Harris, I., Hefner, M., Heinke, J., Houghton, R. A., Hurtt, G. C., Iida, Y., Ilyina, T., Jacobson, A. R., Jain, A., Jarníková, T., Jersild, A., Jiang, F., Jin, Z., Joos, F., Kato, E., Keeling, R. F., Kennedy, D., Klein Goldewijk, K., Knauer, J., Korsbakken, J. I., Körtzinger, A., Lan, X., Lefèvre, N., Li, H., Liu, J., Liu, Z., Ma, L., Marland, G., Mayot, N., McGuire, P. C., McKinley, G. A., Meyer, G., Morgan, E. J., Munro, D. R., Nakaoka, S.-I., Niwa, Y., O'Brien, K. M., Olsen, A., Omar, A. M., Ono, T., Paulsen, M., Pierrot, D., Pocock, K., Poulter, B., Powis, C. M., Rehder, G., Resplandy, L., Robertson, E., Rödenbeck,

https://doi.org/10.5194/egusphere-2026-1898
Preprint. Discussion started: 18 May 2026

C., Rosan, T. M., Schwinger, J., Séférian, R., Smallman, T. L., Smith, S. M., Sospedra-Alfonso, R., Sun, Q., Sutton, A. J., Sweeney, C., Takao, S., Tans, P. P., Tian, H., Tilbrook, B., Tsujino, H., Tubiello, F., van der Werf, G. R., van Ooijen, E., Wanninkhof, R., Watanabe, M., Wimart-Rousseau, C., Yang, D., Yang, X., Yuan, W., Yue, X., Zaehle, S., Zeng, J., and Zheng, B.: Global Carbon Budget 2023, Earth System Science Data, 15, 5301–5369, https://doi.org/10.5194/essd-15-5301-2023, 2023.

Gauch, H. G., Hwang, J. G., and Fick, G. W.: Model evaluation by comparison of model-based predictions and measured values, Agronomy Journal, 95, 1442–1446, 2003.

Gourdji, S. M., Sibley, A. M., and Lobell, D. B.: Global crop exposure to critical high temperatures in the reproductive period: historical trends and future projections, Environmental Research Letters, 8, 024 041, 2013.

Hastie, T. and Pregibon, D.: Generalized linear models, in: Statistical Models in S, edited by Chambers, J. M. and Hastie, T. J., chap. 6, Wadsworth & Brooks/Cole, 1992.

Hemmen, M., Webber, H., von Bloh, W., Heinke, J., and Müller, C.: Model code for GMD submission "Canopy temperatures in computationally expensive crop models: a resource-efficient emulator approach applied in LPJmL (version 5.9.18)", https://doi.org/10.5281/zenodo.18937839, 2026.

Hersbach, H., Bell, B., Berrisford, P., Biavati, G., Horányi, A., Muñoz Sabater, J., Nicolas, J., Peubey, C., Radu, R., Rozum, I., Schepers, D., Simmons, A., Soci, C., Dee, D., and Thépaut, J.-N.: ERA5 hourly data on single levels from 1940 to present, Copernicus Climate Change Service (C3S) Climate Data Store (CDS), (accessed on April 2025), https://doi.org/10.24381/cds.adbb2d47, 2018.

Kim, H.: Global soil wetness project phase 3 atmospheric boundary conditions (experiment 1), Data Integration and Analysis System (DIAS) [data set], https://doi.org/10.20783/DIAS.501, 2017.

Kimball, B., White, J., Wall, G., and Ottman, M.: Infrared-Warmed and Unwarmed Wheat Vegetation Indices Coalesce Using Canopy-Temperature–Based Growing Degree Days, Agronomy Journal, 104, 114–118, 2012.

Kimball, B., White, J., Ottman, M., Wall, G., Bernacchi, C., Morgan, J., and Smith, D.: Predicting canopy temperatures and infrared heater energy requirements for warming field plots, Agronomy Journal, 107, 129–141, 2015.

Lamarque, J.-F., Dentener, F., McConnell, J., Ro, C.-U., Shaw, M., Vet, R., Bergmann, D., Cameron-Smith, P., Dalsoren, S., Doherty, R., et al.: Multi-model mean nitrogen and sulfur deposition from the Atmospheric Chemistry and Climate Model Intercomparison Project (ACCMIP): evaluation of historical and projected future changes, Atmospheric Chemistry and Physics, 13, 7997–8018, 2013.

Lange, S. and Büchner, M.: ISIMIP3b bias-adjusted atmospheric climate input data, https://doi.org/10.48364/ISIMIP.842396.1, 2021.

Lange, S., Quesada-Chacón, D., Mengel, M., Treu, S., and Büchner, M.: ISIMIP3a atmospheric climate input data (v1.3). ISIMIP Repository, https://doi.org/10.48364/ISIMIP.982724.3, 2025.

Li, C., Zwiers, F., Zhang, X., Li, G., Sun, Y., and Wehner, M.: Changes in annual extremes of daily temperature and precipitation in CMIP6 models, Journal of Climate, 34, 3441–3460, 2021.

Lieberei, R., Reisdorff, C., and Franke, W.: Nutzpflanzenkunde, Georg Thieme Verlag, 2007.

Lobell, D. B., Bänziger, M., Magorokosho, C., and Vivek, B.: Nonlinear heat effects on African maize as evidenced by historical yield trials, Nature climate change, 1, 42–45, 2011.

Miller, S., Chua, K., Coggins, J., and Mohtadi, H.: Heat waves, climate change, and economic output, Journal of the European Economic Association, 19, 2658–2694, 2021.

Minoli, S., Egli, D. B., Rolinski, S., and Müller, C.: Modelling cropping periods of grain crops at the global scale, Global and Planetary Change, 174, 35–46, 2019.

Monteith, J. and Unsworth, M.: Principles of Environmental Physics, Edward Arnold, London, 2 edn., 1990.

https://doi.org/10.5194/egusphere-2026-1898
Preprint. Discussion started: 18 May 2026

National Plant Germplasm System, United States Department of Agriculture-Agricultural Research Service: GRIN-Global, https://npgsweb.ars-grin.gov/gringlobal/search, 2025.

Ostberg, S., Müller, C., Heinke, J., and Schaphoff, S.: LandInG 1.0: a toolbox to derive input datasets for terrestrial ecosystem modelling at variable resolutions from heterogeneous sources, Geoscientific Model Development, 16, 3375–3406, 2023.

Ottman, M., Kimball, B., White, J., and Wall, G.: Wheat growth response to increased temperature from varied planting dates and supplemental infrared heating, Agronomy Journal, 104, 7–16, 2012.

Pongsivapai, P., Thongjoo, C., Romkaew, J., and Inboonchuay, T.: Effect of fertilizer management in combination with soil conditioner on yield of cassava cultivated on coarse-textured soil in thailand, Modern Appl Sci, 10, 239–247, 2016.

Porter, J. R. and Gawith, M.: Temperatures and the growth and development of wheat: a review, European journal of agronomy, 10, 23–36, 1999.

Reginato, R. J., Hatfield, J. L., Bauer, A., Hubbard, K. G., Blad, B. L., Verma, S. B., Kanemasu, E. T., and Major, D. J.: Winter wheat response to water and nitrogen in the North American Great Plains, Agricultural and forest meteorology, 44, 105–116, 1988.

Schaphoff, S., Forkel, M., Müller, C., Knauer, J., Von Bloh, W., Gerten, D., Jägermeyr, J., Lucht, W., Rammig, A., Thonicke, K., et al.: LPJmL4–a dynamic global vegetation model with managed land–Part 2: Model evaluation, Geoscientific Model Development, 11, 1377–1403, 2018a.

Schaphoff, S., von Bloh, W., Rammig, A., Thonicke, K., Biemans, H., Forkel, M., Gerten, D., Heinke, J., Jägermeyr, J., Knauer, J., et al.: LPJmL4–a dynamic global vegetation model with managed land–Part 1: Model description, Geoscientific Model Development, 11, 1343–1375, 2018b.

Schlenker, W. and Roberts, M. J.: Nonlinear temperature effects indicate severe damages to US crop yields under climate change, Proceedings of the National Academy of sciences, 106, 15 594–15 598, 2009.

Seneviratne, S. I., Zhang, X., Adnan, M., Badi, W., Dereczynski, C., Luca, A. D., Ghosh, S., Iskandar, I., Kossin, J., Lewis, S., et al.: Weather and climate extreme events in a changing climate, Cambridge University Press, pp. 1513–1766, 2021.

Siebert, S., Ewert, F., Rezaei, E. E., Kage, H., and Graß, R.: Impact of heat stress on crop yield—on the importance of considering canopy temperature, Environmental Research Letters, 9, 044 012, 2014.

Teixeira, E. I., Fischer, G., Van Velthuizen, H., Walter, C., and Ewert, F.: Global hot-spots of heat stress on agricultural crops due to climate change, Agricultural and forest Meteorology, 170, 206–215, 2013.

Venables, W. N. and Ripley, B. D.: Modern Applied Statistics with S, Springer, New York, 4 edn., 2002.

von Bloh, W., Schaphoff, S., Müller, C., Rolinski, S., Waha, K., and Zaehle, S.: Implementing the nitrogen cycle into the dynamic global vegetation, hydrology, and crop growth model LPJmL (version 5.0), Geoscientific Model Development, 11, 2789–2812, 2018.

Waha, K., Van Bussel, L., Müller, C., and Bondeau, A.: Climate-driven simulation of global crop sowing dates, Global Ecology and Biogeography, 21, 247–259, 2012.

Wall, G. W., Kimball, B. A., White, J. W., and Ottman, M. J.: Gas exchange and water relations of spring wheat under full-season infrared warming, Global Change Biology, 17, 2113–2133, 2011.

Wall, G. W., McLain, J. E., Kimball, B. A., White, J. W., Ottman, M. J., and Garcia, R. L.: Infrared warming affects intrarow soil carbon dioxide efflux during vegetative growth of spring wheat, Agronomy Journal, 105, 607–618, 2013.

Wang, E., Martre, P., Zhao, Z., Ewert, F., Maiorano, A., Rötter, R. P., Kimball, B. A., Ottman, M. J., Wall, G. W., White, J. W., et al.: The uncertainty of crop yield projections is reduced by improved temperature response functions, Nature plants, 3, 1–13, 2017.

https://doi.org/10.5194/egusphere-2026-1898
Preprint. Discussion started: 18 May 2026

Webber, H., Ewert, F., Kimball, B., Siebert, S., White, J. W., Wall, G., Ottman, M., Trawally, D., and Gaiser, T.: Simulating canopy temperature for modelling heat stress in cereals, Environmental Modelling & Software, 77, 143–155, 2016.

Webber, H., Martre, P., Asseng, S., Kimball, B., White, J., Ottman, M., Wall, G. W., De Sanctis, G., Doltra, J., Grant, R., et al.: Canopy temperature for simulation of heat stress in irrigated wheat in a semi-arid environment: A multi-model comparison, Field Crops Research, 202, 21–35, 2017.

Webber, H., White, J. W., Kimball, B. A., Ewert, F., Asseng, S., Rezaei, E. E., Pinter Jr, P. J., Hatfield, J. L., Reynolds, M. P., Ababaei, B., et al.: Physical robustness of canopy temperature models for crop heat stress simulation across environments and production conditions, Field Crops Research, 216, 75–88, 2018.

Webber, H., Cooke, D., Wang, C., Asseng, S., Martre, P., Ewert, F., Kimball, B., Hoogenboom, G., Evett, S., Chanzy, A., et al.: Wheat crop models underestimate drought stress in semi-arid and Mediterranean environments, Field Crops Research, 332, 110 032, 2025.

White, J. W., Kimball, B. A., Wall, G. W., Ottman, M. J., and Hunt, L.: Responses of time of anthesis and maturity to sowing dates and infrared warming in spring wheat, Field Crops Research, 124, 213–222, 2011.

Wilkinson, G. and Rogers, C.: Symbolic description of factorial models for analysis of variance, Journal of the Royal Statistical Society Series C: Applied Statistics, 22, 392–399, 1973.

Wirth, S. B., Braun, J., Heinke, J., Ostberg, S., Rolinski, S., Schaphoff, S., Stenzel, F., von Bloh, W., Taube, F., and Müller, C.: Biological nitrogen fixation of natural and agricultural vegetation simulated with LPJmL 5.7. 9, Geoscientific Model Development, 17, 7889–7914, 2024.

Yang, J. and Tian, H.: ISIMIP3a N-deposition input data (v1.2), ISIMIP Repository [data set], https://doi.org/https://doi.org/10.48364/ISIMIP.759077.2, 2022.